Three conserved hydrophobic residues in the CC domain of Pit contribute to its plasma membrane localization and immune induction

Qiong Wang[1, 2, $], Yuying Li[2, 3, $], Ken-ichi Kosami[2, 4, $], Chaochao Liu[5], Jing Li[2, 6], Dan Zhang[1], Daisuke Miki[2], and Yoji Kawano[2, 7, 8]

[1] School of Horticulture and Plant Protection, Yangzhou University, Yangzhou 225009, China

[2] CAS Center for Excellence in Molecular Plant Sciences, Shanghai Center for Plant Stress Biology, Chinese Academy of Sciences, Shanghai 201602, China

[3] Lingnan Guangdong Laboratory of Modern Agriculture, Genome Analysis Laboratory of the Ministry of Agriculture, Agricultural Genomics Institute at Shenzhen, Chinese Academy of Agricultural Sciences, Shenzhen 440307, China

[4] Fruit Tree Research Center, Ehime Research Institute of Agriculture, Forestry and Fisheries, Ehime 791-0112, Japan

[5] School of Biotechnology, Jiangsu University of Science and Technology, Zhenjiang 212021, China

[6] University of Chinese Academy of Sciences, Beijing 100049, China

[7] Kihara Institute for Biological Research, Yokohama City University, Kanagawa 244-0813, Japan

[8] Institute of Plant Science and Resources, Okayama University, Okayama 710-0046, Japan

[$] These authors contributed equally to this work.

Correspondence should be addressed to Yoji Kawano,

Institute of Plant Science and Resources

Okayama University

2-20-1, Chuo, Kurashiki, Okayama 710-0046, Japan

Tel: +81-86-434-1242

E-mail: yoji.kawano@okayama-u.ac.jp

Author emails:

Qiong Wang: wangqiong@yzu.edu.cn

Yuying Li: liyuying@caas.cn

Ken-ichi Kosami: kenichi.kosami.1985@gmail.com

Chaochao Liu: qdliuchaohi@163.com

Jing Li: jingli@psc.ac.cn

Dan Zhang: MZ120201287@yzu.edu.cn

Daisuke Miki: miki@sibs.ac.cn

Yoji Kawano: yoji.kawano@okayama-u.ac.jp

ABSTRACT

Nucleotide-binding leucine-rich repeat (NLR) proteins work as crucial intracellular immune receptors. N-terminal domains of NLRs fall into two groups, namely coiled-coil (CC) and Toll-interleukin 1 receptor (TIR) domains, which play critical roles in signal transduction and disease resistance. However, the activation mechanisms of NLRs, and how their N-termini are involved in immune induction, remain largely unknown. Here, we revealed that the rice NLR Pit self-associates through its CC domain. The CC domain of Pit possesses three conserved hydrophobic residues that are known to be involved in homodimer formation in two NLRs, barley MLA10 and Arabidopsis RPM1. Interestingly, the function of these residues in Pit is different from that in MLA10 and RPM1. Although the three hydrophobic residues are important for Pit-induced disease resistance against rice blast fungus, they do not participate in self-association or in binding to downstream signaling molecules. Based on homology modeling of Pit using the structure of the Arabidopsis NLR ZAR1, we tried to clarify the role of the three conserved hydrophobic residues and found that they are involved in the plasma membrane localization. Our findings provide novel insights for understanding the mechanisms of NLR activation as well as the relationship between subcellular localization and immune induction.

Key words: NLR protein; plasma membrane localization; self-association; effector-triggered immunity; rice

INTRODUCTION

Plants have developed two tiers in their immune system, called pattern-triggered immunity (PTI) and effector-triggered immunity (ETI), to detect invasion by various pathogens (Jones & Dangl, 2006; Dodds & Rathjen, 2010). The initiation of PTI depends on the successful perception of conserved pathogen-associated molecular patterns (PAMPs) by surface-localized pattern recognition receptors (PRRs) (Macho & Zipfel, 2014). Once PTI signaling is activated, it is usually accompanied by a series of immune responses, such as the production of reactive oxygen species (ROS), the expression of pathogenesis-related genes, and the synthesis of antimicrobial phytoalexins and the cell wall component lignin (Bigeard *et al.*, 2015). In general, PTI is sufficient to resist the attack of pathogens. Nevertheless, during evolution, pathogens have acquired the ability to secrete effectors into the apoplast or the plant cytoplasm to counteract the defense of PTI (Cui *et al.*, 2015; Jones *et al.*, 2016). To overcome this invasion, plants have co-evolved ETI as the second tier of the immune system. The majority of genetically characterized disease resistance traits in plants map to genes encoding nucleotide-binding domain and leucine-rich repeat proteins (NLRs). These act as receptors to surveil effectors derived from pathogens and to activate ETI, which includes the hypersensitive response (HR) and ROS production. NLRs share two core domains: a central nucleotide-binding (NB-ARC) domain and a C-terminal leucine-rich repeat (LRR) domain (Cui *et al.*, 2015). The NB-ARC domain is thought to serve as a switch domain in NLRs by controlling nucleotide exchange and hydrolysis, and this nucleotide exchange leads to conformational change and oligomerization of NLRs, resulting in the triggering of ETI (Takken *et al.*, 2006; Maekawa *et al.*, 2011a). Highly variable LRR domains define at least part of the recognition specificity of NLRs to pathogen effector proteins. The N-terminus of NLRs is categorized into two domains, namely a Toll/interleukin-1 receptor (TIR) domain and a coiled-coil (CC) domain, and therefore NLRs are subclassified into TIR-NLRs (TNLs) and CC-NLRs (CNLs). Previous studies have demonstrated that in several NLRs, overexpression of the CC or TIR domain alone has autoactivity to induce cell death, implying that N-terminal CC and TIR domains are important platforms to trigger immune responses (Swiderski *et*

al., 2009; Bernoux *et al.*, 2011; Collier *et al.*, 2011; Maekawa *et al.*, 2011a; Wang *et al.*, 2015). N-terminal CC and TIR domains are now known to play key roles in several functions, including indirect surveillance of pathogen effectors and binding of downstream signaling molecules (Cui *et al.*, 2015; Jones *et al.*, 2016; Kourelis & van der Hoorn, 2018).

Moreover, self (homomers) and non-self (heteromers) oligomerization of N-terminal NLRs are indispensable to trigger ETI (Maekawa *et al.*, 2011a; Williams *et al.*, 2014; Wang *et al.*, 2019a). Structural studies have revealed that TIR domains exhibit a flavodoxin-like fold consisting of five α-helices surrounding a five-strand β-sheet, and at least two different oligomerization interfaces exist among the TIR domains (Chakraborty & Ghosh, 2020). The flax TNL L6 possesses the αD and αE helices (the DE interface) (Bernoux *et al.*, 2011), and a pair of Arabidopsis TNLs, RPS4 and RRS1, have αA and αE helices (the AE interface) (Williams *et al.*, 2014). Interestingly, the *Arabidopsis* TNLs SNC1 and RPP1 have the DE/AE or DE/AE-like interaction interfaces (Zhang *et al.*, 2017; Chakraborty & Ghosh, 2020). Recently, two cryo-electron microscopy (EM) structures of TNLs, *Nicotiana benthamiana* ROQ1 and *Arabidopsis* RPP1, were soloved and they revealed that direct bindings of both TNLs to the corresponding effectors induce TNLs to form tetrameric resistosomes for immune signaling (Ma *et al.*, 2020; Martin *et al.*, 2020). The TIR domains of them bind to each other via two distinct interfaces, AE and BE (equivalent to the BB-loop of other TIR domains). While the first structure of the CC domain of CNLwas revealed as an antiparallel homodimer of barley MLA10 in crystals (Maekawa *et al.*, 2011b). Subsequent studies have proved the CC domains of all the other NLRs including wheat Sr33 and potato Rx behave monomeric proteins with a four-helix bundle conformation (Hao *et al.*, 2013; Casey *et al.*, 2016). Recently, using a cryo-EM, Wang et al. revealed the full length structures of the Arabidopsis CNL ZAR1 in monomeric inactive and transition states as well as the active pentameric ZAR1 resistosome (Wang *et al.*, 2019a). The CC domain of ZAR1 also displays a four-helix bundle conformation. A large portion of the helix α1 (residues 12–44) of the MLA10 CC domain appears to be an important interface for homodimerization. Single mutations in three hydrophobic

residues (I33, L36, and M43) of the helix α1 in MLA10 dramatically decreased self-association as well as binding activity to a downstream signaling molecule, HvWRKY1, resulting in compromised resistance to the pathogenic powdery mildew fungus. The hydrophobicity of these residues is conserved among various CNLs including Arabidopsis RPM1. Triple mutation of the corresponding three hydrophobic residues in RPM1 also leads to a loss of self-association and immune induction activity (El Kasmi *et al.*, 2017). All of the single mutants in three hydrophobic residues show reduced interaction with the small host protein RIN4 (El Kasmi *et al.*, 2017). It is unclear whether these residues are universally involved in self-association or whether their functions differ in each NLR.

Evidence has been accumulating that the subcellular distribution of NLRs is important for their functions. Perception of the fungal effector A10 by MLA10 triggers the nuclear translocation from the cytosol, resulting in interaction between MLA10 and HvWRKY1 in the nucleus to induce defense responses (Shen *et al.*, 2007). The intranuclear activities of the Arabidopsis TNL RPS4 restrict bacterial growth and programmed cell death, and nucleocytoplasmic coordination of RPS4 needs transcriptional resistance reinforcement (Heidrich *et al.*, 2011). The potato CNL Rx1 is located in both the cytoplasm and the nucleus, and the appropriate nucleocytoplasmic distribution of Rx1 is required for full functionality (Slootweg *et al.*, 2010; Tameling *et al.*, 2010). Rx1 activation triggered by effector recognition occurs only in the cytoplasm. The CC domain and the cochaperone SGT contribute to nuclear localization of Rx1, but the LRR domain is associated with cytoplasmic localization. The Arabidopsis CNL RPM1 requires plasma membrane distribution while the potato CNL R3a needs endomembrane localization, and disrupting the proper localization of both NLRs impairs their functions (Gao *et al.*, 2011; Engelhardt *et al.*, 2012). The oligomerization-induced active Arabidopsis ZAR1 complex associates with the plasma membrane (Wang *et al.*, 2019a). Although our knowledge of NLR protein localization has increased in recent years, it is not yet sufficient to understand the mechanisms and significance of the dynamic nature of NLR protein localization or the relationship between subcellular localization and activation states.

We have previously revealed that the small GTPase OsRac1 functions as a molecular switch in rice and plays key roles in both PTI and ETI (Kawano *et al.*, 2010; Akamatsu *et al.*, 2013; Kawano & Shimamoto, 2013; Kawano *et al.*, 2014b). OsRac1 forms immune protein complex(es) directly or indirectly with 16 binding partners such as NADPH oxidase and OsMPK6, thereby leading to the induction of immune responses (Lieberherr *et al.*, 2005; Chen *et al.*, 2010; Akamatsu *et al.*, 2013; Kawano & Shimamoto, 2013; Kawano *et al.*, 2014b; Kosami *et al.*, 2014). OsRac1 acts as a downstream switch molecule for three CNLs, Pit, Pia, and PID3, which all confer resistance to *Magnaporthe oryzae*, implying that OsRac1 is a key signaling switch for rice CNLs (Ono *et al.*, 2001; Kawano *et al.*, 2010; Wang *et al.*, 2018; Zhou *et al.*, 2019). Recently, we clarified how the CNL Pit activates OsRac1. Pit interacts directly with the GDP/GTP exchanger (GEF) protein OsSPK1, which is an activator for OsRac1, through its CC domain (Wang *et al.*, 2018) and also associates with OsRac1 through its NB-ARC domain (Kawano *et al.*, 2010). Both Pit and OsRac1 seem to be posttranslationally modified by a lipid modification, palmitoylation, and these three proteins may form a ternary complex at the plasma membrane to trigger ETI (Ono *et al.*, 2001; Kawano *et al.*, 2014a; Yalovsky, 2015; Wang *et al.*, 2018).

In this study, we clarified the role of the above-mentioned three conserved hydrophobic residues in the CC domain of Pit. Interestingly, the three residues are involved in the plasma membrane localization of Pit, and are indispensable for Pit-mediated disease resistance to rice blast fungus, but do not participate in self-association and binding to its direct signaling molecules OsSPK1 and OsRac1. Collectively, our results shed light on how NLRs trigger immune induction.

RESULTS

Pit self-associates through its CC domain

Since several CNL and TNL proteins have been reported to self-associate (Mestre & Baulcombe, 2006; Ade *et al.*, 2007), we tested whether the rice NLR Pit forms homo-oligomers *in planta*. We transiently co-expressed full-length Pit WT-HA and Pit WT-Myc in *Nicotiana benthamiana* and performed a co-immunoprecipitation (co-IP) assay. When Pit WT-HA was precipitated with anti-HA antibody, Pit WT-Myc co-precipitated but a control GUS-HA did not, indicating that Pit self-associates *in planta* (Figure 1A). Previous studies have demonstrated that the N-terminal CC and TIR domains are important interfaces for homo-oligomerization in NLRs, and that these interactions are indispensable for NLR functions (Maekawa *et al.*, 2011a; Williams *et al.*, 2014). Next, we examined whether Pit self-associates through its CC domain (amino acids 1-140). By using a yeast two-hybrid assay, we found that the CC domain of Pit formed homomers (Figure 1B). Consistent with this observation, self-association between the CC domains of Pit was observed in a co-IP assay in *N. benthamiana* (Figure 1C) and an *in vitro* binding assay (Figure 1D). Taken together, these results indicate that Pit forms homomers through its CC domain.

Three conserved residues do not contribute to self-association of Pit

Although the primary sequences of the N-terminal CC domain of NLRs are dissimilar, three hydrophobic residues (I33, L36, and M43) of the helix α1 in MLA10 are highly conserved among the known CNL proteins including Pit (Maekawa *et al.*, 2011a) (Figure 2A). In MLA10 and RPM1, these three residues are involved in self-association and are indispensable for immune induction (Maekawa *et al.*, 2011b; El Kasmi *et al.*, 2017). I33, L36, and M43 in MLA10 correspond to I34, L37, and L41 in Pit. Our finding that Pit forms homomers through its CC domain raised the possibility that the three conserved hydrophobic residues of Pit also participate in oligomerization and are essential for its function. To test this hypothesis, we built a homology model of the CC domain of Pit using the crystal structure of the CC domain of MLA10 (Maekawa *et al.*, 2011a). Similar to MLA10, the model structure of the CC domain of Pit dimerized

209 through the helix α1 using three hydrophobic residues of I34, L37, and L41 (Figure
210 2B). We generated CC domain Pit mutants in which these three conserved residues
211 were converted to negatively charged glutamic acid, and tested whether they are
212 involved in self-association. Interestingly, both the single mutations (Pit I34, L37, or
213 L41) and the triple mutation of Pit (Pit 3E: Pit I34E L37E L41E) retained self-
214 association ability in an *in vitro* binding assay (Figure 2C), and a consistent result was
215 obtained in a yeast two-hybrid assay (Figures 2D and S1A). We also conducted a co-
216 IP assay in *N. benthamiana* using full-length Pit but could not observe a visible effect
217 on self-association (Figure 2E). Overall, these results indicate that the three
218 hydrophobic residues do not contribute to self-association of Pit.
219
220 **Mutations in the three conserved residues of Pit compromise Pit-mediated**
221 **immune responses**
222 Next, we examined whether the effects of the hydrophobic residue mutants of Pit
223 influenced immune responses. We have previously generated a constitutively active
224 form of Pit, named Pit D485V. Pit D485V is a MHD motif mutant that is able to induce
225 cell death and ROS production in *N. Benthamiana*, probably through the employment
226 of tobacco orthologs of OsRac1 and OsSPK1 as downstream signal transducers because
227 the overexpression of the dominat negative form of OsRac1 suppresses Pit D485V-
228 induced cell death in *N. Benthamiana* (Kawano *et al.*, 2010; Kawano *et al.*, 2014b). The
229 single mutations and the triple mutation in the three hydrophobic residues clearly
230 attenuated Pit D485V-induced cell death (Figures 3A and S1C) and ROS production
231 (Figures 3B, S1B and S1C). We also employed two rice systems to evaluate the Pit
232 mutants. We used a luciferase reporter system to monitor the effect of the Pit mutants on
233 cell death in rice protoplasts. In this system, we transfected the *Pit* mutants with a
234 *luciferase* vector into rice protoplasts and measured the viability of protoplasts based
235 on luminescence. We found that the luciferase activity in cells expressing Pit WT was
236 significantly lower than that in cells expressing control GUS, indicating that Pit WT is
237 autoactive and induces cell death in rice protoplasts (Figure 3C). This Pit WT-induced
238 cell death was abolished by the introduction of the mutations in three conserved

239 hydrophobic residues (Figures 3C and S1D). Next, we tested the effect of the
240 hydrophobic residue mutants of Pit on disease resistance to rice blast fungus. In this
241 experiment, we generated transgenic plants of the susceptible rice cultivar Nipponbare
242 carrying the exogenous *Pit* resistance genes (Figure S2A), and chose the avirulent rice
243 blast fungus *M. oryzae* race 007.0, because Pit-dependent disease resistance has been
244 established between *Pit* and *M. oryzae* race 007.0 (Hayashi *et al.*, 2010). Therefore,
245 Nipponbare is a suitable cultivar to assess transgenes encoding the *Pit* mutants.
246 Nipponbare expressing *Pit* WT displayed shorter lesions induced by *M. oryzae* than did
247 Nipponbare, but this effect was compromised in both single and triple mutants for the
248 three hydrophobic residues (Figures 3D and 3E). We also precisely quantified fungal
249 invasion by measuring the amount of fungal DNA using real-time PCR (Figure 3F).
250 The result of this qPCR was consistent with that of the lesion length comparison,
251 showing that mutation of the three hydrophobic residues perturbed Pit-triggered
252 resistance to avirulent rice blast fungus. Take together, these data indicate that the three
253 hydrophobic residues in the CC domain of Pit are indispensable for Pit-mediated
254 immune responses.
255
256 **Mutations in the three conserved hydrophobic residues abolish Pit-induced**
257 **OsRac1 activation but do not affect the interaction with OsRac1 and OsSPK1**
258 Since the three hydrophobic residue mutations of Pit significantly perturbed Pit-
259 mediated immune responses (Figure 3), we checked the interactions between Pit and its
260 two downstream signaling molecules: the molecular switch of rice immunity OsRac1
261 and its activator OsSPK1 . Pit may form a ternary complex with OsSPK1 and OsRac1
262 at the plasma membrane and activates OsRac1 through OsSPK1 to induce Pit-mediated
263 immunity (Kawano *et al.*, 2010; Wang *et al.*, 2018). We previously mapped the binding
264 region of OsSKP1 in Pit and revealed that a proline-rich motif of the CC domain in Pit
265 (residues 91–95) is required for its binding to OsSPK1 (Wang *et al.*, 2018). Consistent
266 with that finding, there is no visible effect in any of the three hydrophobic residue
267 mutants of Pit on binding to OsSPK1 in a co-IP assay in *N. benthamiana* using the CC
268 domain (Figure 4A) and an *in vitro* binding assay (Figure S2B) and the full-length

polypeptide (Figure S2C) of Pit. Moreover, mutating the three hydrophobic residues of Pit did not change its binding activity to OsRac1, probably because OsRac1 binds to the NB-ARC domain of Pit (Figure 4B) (Kawano *et al.*, 2010). Next, we checked OsRac1 activation by the Pit mutants using a Förster resonance energy transfer (FRET) sensor called Ras and interacting protein chimeric unit (Raichu)-OsRac1 (Wong *et al.*, 2018). In this sensor, intramolecular binding of the active GTP-OsRac1 to CRIB brings CFP closer to Venus, enabling FRET from CFP to Venus when OsRac1 is activated (Wong *et al.*, 2018). The resulting Venus fluorescence represents the activation state of OsRac1 *in vivo*: low and high ratios of Venus/CFP fluorescence correspond to low and high levels of OsRac1 activation, respectively. The ratio of Venus/CFP fluorescence of Raichu-OsRac1 in rice protoplasts expressing Pit D485V was much higher than that in protoplasts expressing a control GUS, indicating that Pit D485V activates OsRac1 in rice protoplasts, but the triple mutant Pit 3E with the D485V mutation failed to trigger this activity (Figures 4C and 4D). Thus, we conclude that Pit 3E retains binding activity to OsSPK1 and OsRac1 but loses the ability of wild-type Pit to trigger OsRac1 activation.

Homology modeling of Pit

From the results of our interaction studies in Figure 2, it appears that the MLA10 structure is not applicable to Pit. The structures of the CC domain of NLRs resolve into two types: MLA10 forms dimers and shows a helix–loop–helix structure (Maekawa *et al.*, 2011a), while Sr33 and Rx display a distinct structure that exhibits a four-helix bundle (Hao *et al.*, 2013; Casey *et al.*, 2016). Recently, Wang et al. solved the structure of the inactive and active states of the full-length CNL ZAR1, which revealed that the N-terminal CC domain of inactivated ZAR1 (PDB code 6J5W, Chain A, 1–113) possesses a four-helix bundle, like Sr33 (PDB code 2NCG) and Rx (PDB code 4M70, Chain A) (Figure 5A), implying that Pit also displays the four-helix bundle (Hao *et al.*, 2013; Casey *et al.*, 2016; Wang *et al.*, 2019b). To test this hypothesis and understand the function of I34, L37, and L41 in Pit, we undertook detailed homology structure modeling of Pit based on the inactive (ADP-bound) and active (dATP-bound) structures

of the NLR ZAR1 (Wang *et al.*, 2019a; Wang *et al.*, 2019b). The model structure of the CC domain of Pit displays a four-helix bundle, and the three hydrophobic residues are buried inside the CC domain (Figure 5B). These residues locate on α-helix 2 (α2) and make hydrophobic contact with α-helix1 (α1) and α-helix 3 (α3), which may enhance the stability of the four-helix bundle. The three hydrophobic residues are conserved in Sr33 (I33, L36, and L40), Rx (L24, F27, and L31), and ZAR1 (L31, L34, and L38), and they also form similar hydrophobic contacts (Casey *et al.*, 2016; El Kasmi *et al.*, 2017) (Figure 5B). In the model structure of the inactive form of Pit, the LRR domain sequesters Pit in a monomeric state (Figure 5C). The CC domain of Pit contacts the helical domain (HD1) and a winged-helix domain (WHD) in the NB-ARC domain, and these interactions may keep the CC domain inactive (Burdett *et al.*, 2019; Wang *et al.*, 2019b).

ZAR1 transitions from a monomeric inactive form to the active form, a wheel-like pentameric resistosome, during immune activation (Wang *et al.*, 2019a; Wang *et al.*, 2019b). Since Pit forms homomers (Figure 1), we also generated a model structure of Pit with reference to the structure of the active form of ZAR1 (Wang *et al.*, 2019a). Superposition of the inactive Pit model structure with one protomer of the active Pit model structure revealed that the conformational change between the active and inactive forms of Pit probably occurs at two regions: around the hinge linking the HD and WHD domains, and in the α1 helix of the CC domain (Figure 6A). In the inactive Pit model structure, the amphipathic α1 helix is buried in the four-helix bundle and interacts with the WHD and LRR domains. In the active Pit model structure, the α1 helix rotates and separates from the four-helix bundle, becoming a fully solvent-exposed α1 helix (Burdett *et al.*, 2019). In the active-form Pit model structure, Pit forms a wheel-like pentamer and all the subdomains of Pit are involved in this oligomerization (Figure 6B). The formation of an α-helical funnel-shaped structure in the CC domain contributes to the oligomerization of Pit and is consistent with the self-association of Pit through its CC domain (Figures 1 and 6B) (Wang *et al.*, 2019a). In the active Pit model structure, I34, L37, and L41 locate on the α2 helix and are buried inside the CC domain, implying that they do not contribute to self-association of the CC domain. This

model structure fits well with the result of our binding assays (Figure 2). Interestingly, the three conserved hydrophobic residues make hydrophobic contacts with V75, I78, and V79 of the α3 helix, which itself forms hydrophobic interactions with isoleucines I500 and L510 in the WHD domain (Figure 6C). The introduction of negatively charged glutamic acid into I34, L37, and L41 of Pit may decrease the molecular packing density between α2 and α3 helices in the CC domain, leading to a weakening of the hydrophobic interactions among the α2 and α3 helices of the CC domain, and the WHD domain. Besides, D77 in the α3 helix also forms a hydrogen bond with K532 in the LRR domain. These interactions appear to provide a foundation when the activated protein oligomerizes via its CC domain to form a functional funnel-shaped structure. We checked whether ZAR1 has these interactions between the CC, WHD, and LRR domains in the active ZAR1 structure, and found that L31 and L34 of the α2 helix make hydrophobic contacts with I75 and L76 of the α3 helix, and L115 and I118 of the α4 helix (Figure 6D). Moreover, hydrogen bonds were predicted to between the α2 helix and WHD (K46 and S413) and between the α3 helix and the LRR domain (E67 and R513, E73 and R533). These structural features of ZAR1 are similar to those of Pit modeling.

Mutations in the three hydrophobic residues of Pit perturb its plasma membrane localization

Next, we checked the localization of the hydrophobic residue mutants of Pit in rice protoplasts. We had previously demonstrated that Pit WT is localized at the plasma membrane, but we now found that introducing single mutations into the three hydrophobic residues compromised Pit's plasma membrane localization (Figure 7A) (Kawano *et al.*, 2010; Kawano *et al.*, 2014a). We further investigated the localization of the hydrophobic residue mutants in *N. benthamiana* and found that Pit WT was well merged with FM4-64, a plasma membrane marker, confirming that Pit WT is localized in the plasma membrane (Figure 7B); in contrast, plasma membrane localization was disrupted in all of the hydrophobic residue mutants. Taken together, these results

indicate that the three conserved hydrophobic residues of Pit are required for its proper plasma membrane localization.

We checked the OsSPK1-binding activity of these Pit mutants by bimolecular fluorescence complementation (BiFC) assay in *N. benthamiana*. Consistent with the results of the binding assays (Figure 4A and 4B), OsSPK1 binding was comparable in the mutants to that in Pit WT (Figure 7C). However, the localization of the Pit–OsSPK1 complex differed between Pit WT and the hydrophobic mutants. Pit WT interacted with OsSPK1 at the plasma membrane, as reported previously (Figure 7C) (Wang *et al.*, 2018), but a large proportion of the complexes between OsSPK1 and the Pit mutants was mislocalized away from the plasma membrane. Finally, we examined complex formation between OsRac1 and the Pit mutants by a BiFC assay and found that the Pit WT-OsRac1 complex was situated at the plasma membrane. Interestingly, none of the mutations in the hydrophobic residues disrupted the Pit-OsRac1 interaction at the plasma membrane (Figure 7D), probably because OsRac1 is anchored there by its lipid modification. Taken together, these results indicate that the three conserved hydrophobic residues of Pit are required for its plasma membrane localization.

DISCUSSION

Several TNLs and CNLs have been reported to self-associate through their N-terminal CC or TIR domains; hence, self-association via their N-termini appears to be a general feature of NLRs (Ade *et al.*, 2007; Maekawa *et al.*, 2011a; El Kasmi *et al.*, 2017). Here, we found that the rice blast resistance protein Pit also self-associates through at least its CC domain (Figure 1). Full-length Pit forms homomers in the absence of a pathogen effector, suggesting that it may self-associate before activation and behave like other NLRs, such as RPM1, RPS5, and MLA (Ade *et al.*, 2007; El Kasmi *et al.*, 2017). Previous biophysical analyses have shown that MLA10 is a monomer in solutions but has a dimeric helix-loop-helix structure in crystals (Maekawa *et al.*, 2011a; Casey *et al.*, 2016). It is possible that the dimeric helix-loop-helix structure of MLA10 occurs under the special condition because MLA10 is predominantly monomeric in solution and its character in solution is different from that in the crystals (Casey *et al.*, 2016; Bentham

388 *et al.*, 2018; Burdett *et al.*, 2019). Moreover, the CC domain structures of all other NLRs,
389 including Rx, Sr33, and ZAR1, exhibit a four-helix bundle structure (Casey *et al.*, 2016;
390 El Kasmi *et al.*, 2017; Wang *et al.*, 2019a). Single mutations in the hydrophobic
391 residues (I33, L36, and M43) of α1 helix of MLA10 markedly suppressed self-
392 association, resulting in compromised resistance to *Blumeria graminis* f. sp. *hordei*.
393 We found that introducing the single and triple mutations into Pit did not affect
394 homomer formation, indicating that these residues make at most a marginal
395 contribution to self-association (Figure 2). It is possible that Pit displays a four-helix
396 bundle structure, similar to other NLRs such as Rx, Sr33, and ZAR1. We attempted to
397 clarify the structure of the CC domain of Pit and produced an expression system for the
398 CC domain and full-length Pit protein using *E. coli* and insect cells, but we were unable
399 to obtain intact Pit proteins due to difficulties in expression. The structural analysis of
400 the Pit CC domain will be a topic for future research.

401 Several CNLs, including RPM1 (Gao *et al.*, 2011), RPS2 (Axtell & Staskawicz,
402 2003), RPS5 (Qi *et al.*, 2012), and Tm-2^2 (Chen *et al.*, 2017), have been reported to be
403 localized in the plasma membrane, and this localization is indispensable for their
404 immune induction. RPM1 appears to anchor to the plasma membrane through the plant
405 guardee protein RIN4, which is localized to the membrane via palmitoylation (Kim *et*
406 *al.*, 2005). Two lipid modifications, myristoylation, and palmitoylation, in the CC
407 domain of RPS5, participate in its plasma localization, protein stability, and function in
408 an additive manner. We have previously revealed that a free N-terminus of Pit is
409 required for its function because the N-terminal fusion of GFP compromises cell death
410 activity (Kawano *et al.*, 2014a). Consistent with this, Pit has two palmitoylation sites in
411 its CC domain, which play a key role in the plasma membrane localization of Pit
412 (Kawano *et al.*, 2014a). The resting Pit is localized exclusively in the plasma membrane
413 (Figure 7) (Kawano *et al.*, 2014a), indicating that plasma membrane localization alone
414 is not sufficient to trigger activation. The plasma membrane localization of Pit is ATP-
415 binding activity-dependent because the P-loop mutant of Pit K203R is mislocalized
416 (Kawano *et al.*, 2010). This feature is similar to other CNLs, including RPM1, TM-22,

and RPS5, whose auto active mutants are primarily localized to the plasma membrane (Qi *et al.*, 2012; Chen *et al.*, 2017; El Kasmi *et al.*, 2017).

Recently, the structures of active and inactive forms of ZAR1 have been reported, revealing a more detailed structural observation of the NLR protein. Inactive ZAR1 forms a monomeric complex with resistance-related kinase (RKS1). *Xanthomonas campestris* pv. *campestris* AvrAC uridylates the PBS1-like protein 2 (PBL2) kinase to produce PBL2UMP, which triggers the pentameric ZAR1–RKS1–PBL2UMP resistosome *in vitro* and *in vivo* (Wang *et al.*, 2019a; Wang *et al.*, 2019b; Hu *et al.*, 2020). Resistosome formation is required for AvrAC-triggered cell death and disease resistance. The *Pseudomonas syringae* effector HopZ1a also induces the oligomerization of ZAR1 *in vivo* (Hu *et al.*, 2020). During the transition from the inactive to the active states of ZAR1, positional translation through unfolding and refolding in the a4 helix allows the α1 helix to be released from the four-helix bundle (Wang *et al.*, 2019a). This conformational change of the α1 helix leads to the pentameric funnel-shaped structure of the CC domain of ZAR1. The funnel-shaped structure of active ZAR1 is similar to previously characterized pore-forming proteins, such as mixed lineage kinase-like (MLKL) and hemolytic actinoporin fragaceatoxin C (FraC) (Tanaka *et al.*, 2015). Notably, FraC showed a similar conformational change during pore formation to that upon the activation of ZAR1. The N-terminal helix of FraC is released from the monomer and is capable of forming a funnel-shaped octamer, leading to its insertion into the cell membrane. The structure of the ZAR1 oligomer implies that the funnel structure of the CC domain of the ZAR1 oligomer also inserts into the cell membrane and induces cell death (Wang *et al.*, 2019a). It appears that a funnel-shaped structure participates in membrane localization (Adachi *et al.*, 2019). Recently, Adachi et al. found the consensus sequence called MADA motif in the N-termini of various CNLs which matches the N-terminal α1 helix of ZAR1. They predicted three residues mapped to the outer surface of the funnel-shaped structure of NRC4 based on the ZAR1 resistosome structure and substituted these three hydrophobic residues for negatively charged Glu residues. Those mutants failed to trigger cell death in *N. benthamiana* and one of the mutants decreased its plasma

membrane localization, showing the general importance of insertion of α1 helix of CNLs into plasma membrane on their immunity. Since the membrane localization of Pit is also important for its function (Kawano *et al.*, 2014a), it is possible that the CC domain of Pit has a funnel-shaped structure similar to that of active ZAR1 and plays an important role in its membrane localization and cell death. Our experiments showed that Pit I34E, L37E, and L41E mutants perturbed membrane localization and were localized in the cytoplasm (Figure 7A, B). In the active Pit model structure based on the active ZAR1 (PDB code 6J5T), the three hydrophobic residues (I34, L37, and L41) are located in the α2 helix but not in the α1 helix of the funnel-shaped structure, suggesting that the three hydrophobic residues are not directly involved in membrane insertion. The three hydrophobic residues, I34, L37, and L41, in the α2 helix of the Pit CC domain interact hydrophobically with V75, I78, and V79 in the α3 helix. The α3 helix is hydrophobically associated with I500 in the WHD domain and L510 in the LRR domain (Figure 6C). In addition, D77 in the α3 helix also forms a hydrogen bond with K532 in the LRR domain (Figure 6C). D77 is located at the EDVID motif in Pit (DDIVD in Pit) which is a highly conseved motif in CNLs (Bai *et al.*, 2002). The EDVID motif directly contacts with LRR domain in the inactive ZAR1 structure (Burdett *et al.*, 2019; Wang *et al.*, 2019a). In the full-length MLA10 protein, the mutations of the EDVID motif in MLA10 weaken immune response but the same mutations in the CC domain fragment do not affect its autoactivity (Bai et al., 2012), suggesting that the EDVID motif is necessary for both autoinhibition and activation of MLA10. Like the ZAR1 case, it is possible that the EDVID motif serves as a signal relay from the LRR domain to the CC domain to indue the large conformational changes in the NB-LRR region. The three hydrophobic residues (I34, L37, and L41) in the α2 helix may support the funnel-shaped structure through interaction with the α3 helix, which is associated with the WHD and LRR domains. However, the substitutions of I34, L37, and L41 with Glu may destabilize this foundation for the funnel-shaped structure and consequently affect the insertion of the funnel-shaped structure formed by the N-terminal α1 helix into the membrane. Alternatively, we previously found that palmitoylation is required for plasma membrane localization of Pit (Kawano *et al.*,

2014a) and these mutations in the CC domain of Pit may affect appropriate palmitoylation. But these speculations need to be tested in the future. The mislocalization of Pit by the mutations into the conserved hydrophobic residues disrupted the appropriate localization of the Pit-OsSPK1 complex (Figure 7C). This may lead to the attenuation of Pit-mediated immune responses.

Author Contributions

Q. W. and Y. K. designed the study; Q. W., Y. L., K. K., J. L., D. Z., and Y. K. performed experiments and analyzed data; Q. W., K. K., and Y. K. wrote the manuscript; C. L. and D. M. gave technical support; Y. K. provided conceptual advice.

Competing financial interests

The authors declare that they have no competing financial interests.

References

Adachi H, Contreras MP, Harant A, Wu CH, Derevnina L, Sakai T, Duggan C, Moratto E, Bozkurt TO, Maqbool A, et al. 2019. An N-terminal motif in NLR immune receptors is functionally conserved across distantly related plant species. *Elife* **8**.

Ade J, DeYoung BJ, Golstein C, Innes RW. 2007. Indirect activation of a plant nucleotide binding site-leucine-rich repeat protein by a bacterial protease. *Proc Natl Acad Sci U S A* **104**(7): 2531-2536.

Akamatsu A, Wong H, Fujiwara M, Okuda J, Nishide K, Uno K, Imai K, Umemura K, Kawasaki T, Kawano Y, et al. 2013. An OsCEBiP/OsCERK1-OsRacGEF1-OsRac1 module is an essential component of chitin-induced rice immunity. *Cell Host Microbe* **13**(4): 465-476.

Axtell MJ, Staskawicz BJ. 2003. Initiation of RPS2-specified disease resistance in Arabidopsis is coupled to the AvrRpt2-directed elimination of RIN4. *Cell* **112**(3): 369-377.

Bai J, Pennill LA, Ning J, Lee SW, Ramalingam J, Webb CA, Zhao B, Sun Q, Nelson JC, Leach JE, et al. 2002. Diversity in nucleotide binding site-leucine-rich repeat genes in cereals. *Genome Res* **12**(12): 1871-1884.

Bentham AR, Zdrzalek R, De la Concepcion JC, Banfield MJ. 2018. Uncoiling CNLs: Structure/Function Approaches to Understanding CC Domain Function in Plant NLRs. *Plant Cell Physiol* **59**(12): 2398-2408.

Bernoux M, Ve T, Williams S, Warren C, Hatters D, Valkov E, Zhang X, Ellis JG, Kobe B, Dodds PN. 2011. Structural and functional analysis of a plant resistance protein TIR domain reveals interfaces for self-association, signaling, and autoregulation. *Cell Host Microbe* **9**(3): 200-211.

Bigeard J, Colcombet J, Hirt H. 2015. Signaling mechanisms in pattern-triggered immunity (PTI). *Mol Plant* **8**(4): 521-539.

Burdett H, Bentham AR, Williams SJ, Dodds PN, Anderson PA, Banfield MJ, Kobe B. 2019. The Plant "Resistosome": Structural Insights into Immune Signaling. *Cell Host Microbe* **26**(2): 193-201.

Casey LW, Lavrencic P, Bentham AR, Cesari S, Ericsson DJ, Croll T, Turk D, Anderson PA, Mark AE, Dodds PN, et al. 2016. The CC domain structure from the wheat stem rust resistance protein Sr33 challenges paradigms for dimerization in plant NLR proteins. *Proc Natl Acad Sci U S A* **113**(45): 12856-12861.

Chakraborty J, Ghosh P. 2020. Advancement of research on plant NLRs evolution, biochemical activity, structural association, and engineering. *Planta* **252**(6): 101.

Chen L, Hamada S, Fujiwara M, Zhu T, Thao NP, Wong HL, Krishna P, Ueda T, Kaku H, Shibuya N, et al. 2010. The Hop/Sti1-Hsp90 chaperone complex facilitates the maturation and transport of a PAMP receptor in rice innate immunity. *Cell Host Microbe* **7**(3): 185-196.

Chen T, Liu D, Niu X, Wang J, Qian L, Han L, Liu N, Zhao J, Hong Y, Liu Y. 2017. Antiviral Resistance Protein Tm-2(2) Functions on the Plasma Membrane. *Plant Physiol* **173**(4): 2399-2410.

Collier SM, Hamel LP, Moffett P. 2011. Cell death mediated by the N-terminal domains of a unique and highly conserved class of NB-LRR protein. *Mol Plant Microbe Interact*

24(8): 918-931.

Cui H, Tsuda K, Parker JE. 2015. Effector-triggered immunity: from pathogen perception to robust defense. *Annu Rev Plant Biol* **66**: 487-511.

Dodds PN, Rathjen JP. 2010. Plant immunity: towards an integrated view of plant-pathogen interactions. *Nat Rev Genet* **11**(8): 539-548.

El Kasmi F, Chung EH, Anderson RG, Li J, Wan L, Eitas TK, Gao Z, Dangl JL. 2017. Signaling from the plasma-membrane localized plant immune receptor RPM1 requires self-association of the full-length protein. *Proc Natl Acad Sci U S A* **114**(35): E7385-E7394.

Engelhardt S, Boevink PC, Armstrong MR, Ramos MB, Hein I, Birch PR. 2012. Relocalization of late blight resistance protein R3a to endosomal compartments is associated with effector recognition and required for the immune response. *Plant Cell* **24**(12): 5142-5158.

Gao Z, Chung EH, Eitas TK, Dangl JL. 2011. Plant intracellular innate immune receptor Resistance to Pseudomonas syringae pv. maculicola 1 (RPM1) is activated at, and functions on, the plasma membrane. *Proc Natl Acad Sci U S A* **108**(18): 7619-7624.

Hao W, Collier SM, Moffett P, Chai J. 2013. Structural basis for the interaction between the potato virus X resistance protein (Rx) and its cofactor Ran GTPase-activating protein 2 (RanGAP2). *J Biol Chem* **288**(50): 35868-35876.

Hayashi K, Yasuda N, Fujita Y, Koizumi S, Yoshida H. 2010. Identification of the blast resistance gene Pit in rice cultivars using functional markers. *Theor Appl Genet* **121**(7): 1357-1367.

Hayashi K, Yoshida H. 2009. Refunctionalization of the ancient rice blast disease resistance gene Pit by the recruitment of a retrotransposon as a promoter. *Plant J* **57**(3): 413-425.

Heidrich K, Wirthmueller L, Tasset C, Pouzet C, Deslandes L, Parker JE. 2011. Arabidopsis EDS1 connects pathogen effector recognition to cell compartment-specific immune responses. *Science* **334**(6061): 1401-1404.

Hu M, Qi J, Bi G, Zhou JM. 2020. Bacterial Effectors Induce Oligomerization of Immune Receptor ZAR1 In Vivo. *Mol Plant* **13**(5): 793-801.

Jones JD, Dangl JL. 2006. The plant immune system. *Nature* **444**(7117): 323-329.

Jones JD, Vance RE, Dangl JL. 2016. Intracellular innate immune surveillance devices in plants and animals. *Science* **354**(6316).

Kawano Y, Akamatsu A, Hayashi K, Housen Y, Okuda J, Yao A, Nakashima A, Takahashi H, Yoshida H, Wong HL, et al. 2010. Activation of a Rac GTPase by the NLR family disease resistance protein Pit plays a critical role in rice innate immunity. *Cell Host Microbe* **7**(5): 362-375.

Kawano Y, Fujiwara T, Yao A, Housen Y, Hayashi K, Shimamoto K. 2014a. Palmitoylation-dependent membrane localization of the rice resistance protein pit is critical for the activation of the small GTPase OsRac1. *J Biol Chem* **289**(27): 19079-19088.

Kawano Y, Kaneko-Kawano T, Shimamoto K. 2014b. Rho family GTPase-dependent immunity in plants and animals. *Front Plant Sci* **5**: 522.

Kawano Y, Shimamoto K. 2013. Early signaling network in rice PRR- and R-mediated immunity. *Curr Opin Plant Biol* **16**: 496–504.

Kim HS, Desveaux D, Singer AU, Patel P, Sondek J, Dangl JL. 2005. The Pseudomonas

580 syringae effector AvrRpt2 cleaves its C-terminally acylated target, RIN4, from
581 Arabidopsis membranes to block RPM1 activation. *Proc Natl Acad Sci U S A* **102**(18):
582 6496-6501.
583 **Kosami K, Ohki I, Nagano M, Furuita K, Sugiki T, Kawano Y, Kawasaki T, Fujiwara T,**
584 **Nakagawa A, Shimamoto K, et al. 2014.** The crystal structure of the plant small
585 GTPase OsRac1 reveals its mode of binding to NADPH oxidase. *J Biol Chem* **289**(41):
586 28569-28578.
587 **Kourelis J, van der Hoorn RAL. 2018.** Defended to the Nines: 25 Years of Resistance Gene
588 Cloning Identifies Nine Mechanisms for R Protein Function. *Plant Cell* **30**(2): 285-299.
589 **Lieberherr D, Thao NP, Nakashima A, Umemura K, Kawasaki T, Shimamoto K. 2005.** A
590 sphingolipid elicitor-inducible mitogen-activated protein kinase is regulated by the
591 small GTPase OsRac1 and heterotrimeric G-protein in rice. *Plant Physiol* **138**(3):
592 1644-1652.
593 **Ma S, Lapin D, Liu L, Sun Y, Song W, Zhang X, Logemann E, Yu D, Wang J, Jirschitzka**
594 **J, et al. 2020.** Direct pathogen-induced assembly of an NLR immune receptor complex
595 to form a holoenzyme. *Science* **370**(6521).
596 **Macho AP, Zipfel C. 2014.** Plant PRRs and the activation of innate immune signaling. *Mol*
597 *Cell* **54**(2): 263-272.
598 **Maekawa T, Cheng W, Spiridon LN, Toller A, Lukasik E, Saijo Y, Liu P, Shen QH, Micluta**
599 **MA, Somssich IE, et al. 2011a.** Coiled-coil domain-dependent homodimerization of
600 intracellular barley immune receptors defines a minimal functional module for
601 triggering cell death. *Cell Host Microbe* **9**(3): 187-199.
602 **Maekawa T, Cheng W, Spiridon LN, Toller A, Lukasik E, Saijo Y, Liu P, Shen QH, Micluta**
603 **MA, Somssich IE, et al. 2011b.** Coiled-coil domain-dependent homodimerization of
604 intracellular barley immune receptors defines a minimal functional module for
605 triggering cell death. *Cell Host Microbe* **9**(3): 187-199.
606 **Martin R, Qi T, Zhang H, Liu F, King M, Toth C, Nogales E, Staskawicz BJ. 2020.** Structure
607 of the activated ROQ1 resistosome directly recognizing the pathogen effector XopQ.
608 *Science* **370**(6521).
609 **Mestre P, Baulcombe DC. 2006.** Elicitor-mediated oligomerization of the tobacco N disease
610 resistance protein. *Plant Cell* **18**(2): 491-501.
611 **Ono E, Wong HL, Kawasaki T, Hasegawa M, Kodama O, Shimamoto K. 2001.** Essential
612 role of the small GTPase Rac in disease resistance of rice. *Proc Natl Acad Sci U S A*
613 **98**(2): 759-764.
614 **Qi D, DeYoung BJ, Innes RW. 2012.** Structure-function analysis of the coiled-coil and leucine-
615 rich repeat domains of the RPS5 disease resistance protein. *Plant Physiol* **158**(4): 1819-
616 1832.
617 **Shen QH, Saijo Y, Mauch S, Biskup C, Bieri S, Keller B, Seki H, Ulker B, Somssich IE,**
618 **Schulze-Lefert P. 2007.** Nuclear activity of MLA immune receptors links isolate-
619 specific and basal disease-resistance responses. *Science* **315**(5815): 1098-1103.
620 **Slootweg E, Roosien J, Spiridon LN, Petrescu AJ, Tameling W, Joosten M, Pomp R, van**
621 **Schaik C, Dees R, Borst JW, et al. 2010.** Nucleocytoplasmic distribution is required
622 for activation of resistance by the potato NB-LRR receptor Rx1 and is balanced by its
623 functional domains. *Plant Cell* **22**(12): 4195-4215.

Swiderski MR, Birker D, Jones JD. 2009. The TIR domain of TIR-NB-LRR resistance proteins is a signaling domain involved in cell death induction. *Mol Plant Microbe Interact* **22**(2): 157-165.

Takken FL, Albrecht M, Tameling WI. 2006. Resistance proteins: molecular switches of plant defence. *Curr Opin Plant Biol* **9**(4): 383-390.

Tameling WI, Nooijen C, Ludwig N, Boter M, Slootweg E, Goverse A, Shirasu K, Joosten MH. 2010. RanGAP2 mediates nucleocytoplasmic partitioning of the NB-LRR immune receptor Rx in the Solanaceae, thereby dictating Rx function. *Plant Cell* **22**(12): 4176-4194.

Tanaka K, Caaveiro JM, Morante K, Gonzalez-Manas JM, Tsumoto K. 2015. Structural basis for self-assembly of a cytolytic pore lined by protein and lipid. *Nat Commun* **6**: 6337.

Wang GF, Ji J, El-Kasmi F, Dangl JL, Johal G, Balint-Kurti PJ. 2015. Molecular and functional analyses of a maize autoactive NB-LRR protein identify precise structural requirements for activity. *PLoS Pathog* **11**(2): e1004674.

Wang J, Hu M, Wang J, Qi J, Han Z, Wang G, Qi Y, Wang HW, Zhou JM, Chai J. 2019a. Reconstitution and structure of a plant NLR resistosome conferring immunity. *Science* **364**(6435).

Wang J, Wang J, Hu M, Wu S, Qi J, Wang G, Han Z, Qi Y, Gao N, Wang HW, et al. 2019b. Ligand-triggered allosteric ADP release primes a plant NLR complex. *Science* **364**(6435): 43.

Wang Q, Li Y, Ishikawa K, Kosami KI, Uno K, Nagawa S, Tan L, Du J, Shimamoto K, Kawano Y. 2018. Resistance protein Pit interacts with the GEF OsSPK1 to activate OsRac1 and trigger rice immunity. *Proc Natl Acad Sci U S A* **115**(49): E11551-E11560.

Williams SJ, Sohn KH, Wan L, Bernoux M, Sarris PF, Segonzac C, Ve T, Ma Y, Saucet SB, Ericsson DJ, et al. 2014. Structural basis for assembly and function of a heterodimeric plant immune receptor. *Science* **344**(6181): 299-303.

Wong HL, Akamatsu A, Wang Q, Higuchi M, Matsuda T, Okuda J, Kosami KI, Inada N, Kawasaki T, Kaneko-Kawano T, et al. 2018. In vivo monitoring of plant small GTPase activation using a Forster resonance energy transfer biosensor. *Plant Methods* **14**: 56.

Yalovsky S. 2015. Protein lipid modifications and the regulation of ROP GTPase function. *J Exp Bot* **66**(6): 1617-1624.

Zhang X, Bernoux M, Bentham AR, Newman TE, Ve T, Casey LW, Raaymakers TM, Hu J, Croll TI, Schreiber KJ, et al. 2017. Multiple functional self-association interfaces in plant TIR domains. *Proc Natl Acad Sci U S A* **114**(10): E2046-E2052.

Zhou Z, Pang Z, Zhao S, Zhang L, Lv Q, Yin D, Li D, Liu X, Zhao X, Li X, et al. 2019. Importance of OsRac1 and RAI1 in signalling of NLR protein-mediated resistance to rice blast disease. *New Phytol*.

667 **FIGURE LEGENDS**

668 **Figure 1. The CC domain and full-length Pit self-associate**

669 **A**, Co-IP assay to assess self-association of full-length Pit in *N. benthamiana*. Total
670 protein extract was immunoprecipitated with anti-HA antibody, and western blotting
671 was then carried out with anti-HA and anti-Myc antibodies. **B**, Yeast two-hybrid assay
672 to test self-association of the Pit CC domain. Growth of yeast cells coexpressing GAL4-
673 AD or GAL4-BD fused with the CC domain of Pit on selective medium without
674 histidine (-His) represents a positive interaction. AD: GAL4 activation domain, BD:
675 GAL4 DNA-binding domain. **C**, Co-IP assay to assess self-association of the Pit CC
676 domain in *N. benthamiana*. Total protein extract was immunoprecipitated with anti-
677 GFP antibody, and western blotting was then carried out with anti-GFP and anti-Myc
678 antibodies. **D**, GST pull-down assay to verify the self-association of the Pit CC domain.
679 Purified GST or GST-tagged Pit CC immobilized on Sepharose was incubated with His-
680 SUMO-tagged Pit CC. After washing, the bound proteins were eluted by addition of
681 SDS loading buffer for immunoblotting with anti-GST and anti-SUMO.

682

683 **Figure 2. Conserved hydrophobic residues in the Pit CC domain are not involved**
684 **in Pit self-association**

685 **A**, Multiple alignment of Pit with various CNLs. **B**, Model structure of the Pit CC
686 domain, based on the MLA10 CC domain (Protein Data Bank ID code 3QFL), shows
687 the elongated dimer (blue and pink), stabilized by hydrophobic residues (I34, L37, and
688 L41). The figure was drawn using PyMOL. **C**, *In vitro* pull-down assay to test the self-
689 association of Pit CC mutants. Purified GST or GST-tagged Pit CC mutants
690 immobilized on Sepharose was incubated with His-SUMO-tagged Pit CC mutants.
691 After washing, the bound proteins were eluted by addition of SDS loading buffer for
692 immunoblotting. Anti-GST and anti-SUMO antibodies were used for western blotting.
693 **D**, Yeast two-hybrid assay to test self-association of Pit CC mutants. Growth of yeast
694 cells coexpressing GAL4-AD or GAL4-BD fused with the CC domain of Pit on
695 selective medium (-LWHA) represents a positive interaction. 10^{-1}, 10^{-2}, and 10^{-3}
696 indicate dilution ratio. **E**, Co-IP assay to examine self-association of full-length Pit

mutants in *N. benthamiana*. Total protein extract was immunoprecipitated with anti-GFP antibody, and western blottingwas then carried out with anti-GFP and anti-Myc antibodies. The post-transfer membrane was stained with Ponceau S.

Figure 3. Conserved hydrophobic residues in the Pit CC domain contribute to Pit-mediated immune signaling

A, Cell death phenotypes induced by transient expression of Pit mutants in *N. benthamiana*. Photos were taken at 2 dpi. The circles indicate the infiltrated regions. **B**, Effect of three hydrophobic residues on Pit D485V-induced ROS production in *N. benthamiana*. ROS production was examined by DAB staining at 2 dpi. **C**, Cell death activity of Pit mutants in rice protoplasts. Relative luciferase activity (GUS=100) is shown. Data are expressed as mean ± standard error (SE) (**$P < 0.01$, $n = 3$). **D** and **E**, Responses, in plants overexpressing Pit WT or mutants, to infection with the incompatible *M. oryzae* race 007.0. **D**, Photograph shows typical phenotypes of transgenic and WT plants at 7 dpi. **E**, Statistical analysis of lesion length was performed at 6 dpi. Relative lesion length [Nippobnare (NB) = 1] is shown. Data are expressed as mean ± standard error (SE) (*$P < 0.05$; $n \geq 30$). **F**, Growth of the incompatible *M. oryzae* race in Nipponbare wild-type plants and transgenic plants overexpressing Pit WT or mutants. Relative infection ratio (NB = 1) is shown. Data are expressed as mean ± standard error (SE) (*$P < 0.05$; **$P < 0.01$; $n = 10$).

Figure 4. Mutations in three hydrophobic residues do not affect binding to OsSPK1 or OsRac1 but perturb Pit-mediated OsRac1 activation

A, Co-IP to test the interaction between OsSPK1 and Pit hydrophobic residue mutants in *N. benthamiana*. Total protein extract was immunoprecipitated with anti-GFP antibody, and western blotting was then carried out with anti-GFP and anti-HA antibodies. The post-transfer membrane was stained with Ponceau S. **B**, Co-IP to test the interaction between OsRac1 and Pit hydrophobic residue mutants in *N. benthamiana*. Total protein extract was immunoprecipitated with anti-GFP antibody, and western blotting was then carried out with anti-GFP and anti-Myc antibodies. The

post-transfer membrane was stained with Ponceau S. **C** and **D**, *In vivo* OsRac1 activation by Pit hydrophobic residues mutants. **C**, Emission ratio images of confocal laser-scanning micrographs of rice protoplasts coexpressing Raichu-OsRac1 and the indicated Pit mutants, or negative control GUS. Scale bars, 5 μm. **D**, Quantification of normalized emission ratios of Venus to CFP. Data are expressed as mean ± standard error (SE) (**$P < 0.01$, $n = 60$).

Figure 5. The CC domain of various NLRs

A, The main chains of the CC domain structure of Sr33 (blue, solution NMR condition, Protein Data Bank ID code 2NCG), Rx (light blue, crystal condition, Protein Data Bank ID code 4M70), and inactivated ZAR1 (orange, electron microscopy condition, 6J5W, residues 1–113) were superimposed using PyMOL. **B,** Comparison of conserved hydrophobic residues of Pit (residues 1–115), inactivated ZAR1 (residues 1–113), Sr33, and Rx. The side chains of three key hydrophobic residues in Pit (I34, L37, and L41) and equivalent residues in inactivated ZAR1 1–113 (L31, L34, and L38), Rx (I33, L36, and L40), Sr33 (L24, F27, and L31), as well as the side chains of amino acids thought to be involved in hydrophobic interactions with these three residues, are shown in stick representation. **C,** Model structure and domain composition of full-length Pit, based on inactivated ZAR1 (Protein Data Bank ID code 6J5W), shows the monomeric state. The figure was drawn using PyMOL.

Figure 6. Homology modeling of Pit using activated ZAR1 as a template

A, Comparison of the inactivated and activated Pit model structures. The model structures of inactivated and activated Pit are based on the structures of inactivated ZAR1 (Protein Data Bank ID code 6J5W) and activated ZAR1 (Protein Data Bank ID code 6J5T). Conformational changes (black arrows) between the activated and inactivated forms of Pit occur around the hinge linking the HD domain (blue) and WHD domain (pink) of Pit and also at the α1 helix of the CC domain (orange). **B,** Model structure of the activated Pit pentamer. The extreme N-terminal α1 helix of the Pit pentamer may be required for the plasma membrane association of Pit. The CC, NBD,

HD1, WHD, and LRR domains are shown in orange, green, blue, pink, and yellow, respectively. **C,** Hydrophobic interactions among α2 (I34, L37, and L41), α3 (F73, V75, I78, and V79), and WHD domain (I500 and L510) in the activated Pit pentamer model structure are shown. Residues that may be important for hydrophobic interactions in Pit function are shown in green, and hydrogen-bonded side chains are shown in light blue. **D,** Comparison of the interaction around α1 of the activated ZAR1 structure (Protein Data Bank ID code 6J5T) and the active Pit oligomer model structure. Residues involved in hydrophobic interaction around α1 are shown in green, and hydrogen-bonded side chains are shown in light blue. The figure was drawn using PyMOL.

Figure 7. Mutations in the conserved hydrophobic residues of Pit influence its plasma membrane localization

A and **B**, Subcellular localization of Pit mutants in rice protoplasts and *N. benthamiana* leaves. **A**, Rice protoplasts were cotransfected with the indicated *Pit-Venus* mutants and *OsFLS2-mCherry.* Scale bars, 5 μm. **B**, Tobacco leaves were injected with *Agrobacterium* carrying *Pit-GFP* mutants (green) and stained with FM4-64 (red: plasma membrane marker). Enlarged images of the boxed areas are shown in the right panels. Scale bars, 25 μm. **C** and **D**, BiFC to detect interactions between Pit hydrophobic residue mutants and OsSPK1 (**C**) or OsRac1 (**D**). Expression constructs were transiently expressed in *N. benthamiana* after agroinfiltration. Empty vector served as a negative control. FM4-64 was used as a plasma membrane marker. Images were captured at 45 h post-infiltration. Enlarged images of the boxed areas in (C) are shown in the right panels. Scale bars, 25 μm.

EXPERIMENTAL PROCEDURES

Plasmid Construction

For Gateway system-constructed plasmids, the target genes and fragments were first cloned into the pENTR/D-TOPO vector (Invitrogen), and then transferred by LR reaction into multiple destination vectors depending on the experimental requirements. For site-directed mutagenesis, overlapping PCR amplification using site-specific and mutagenic primers and pENTR templates was employed to generate *Pit* mutants. For pull-down and yeast two-hybrid assays, *Pit* mutants were directly cloned into the 6×His-SUMO, pGADT7, and pGBKT7 vectors, using restriction enzymes and T4 ligase (New England Biolabs).

Yeast Two-Hybrid Assay

The Y2HGold-GAL4 system was used to test interactions between target proteins by transforming GAL4-AD/BD fused *Pit* plasmids into Y2HGold chemically competent cells (Weidibio: YC1002).

Transient Expression and HR Assays

Agroinfiltration of *N. benthamiana* was conducted as described previously (Kawano *et al.*, 2010). *Agrobacterium tumefaciens* strain GV3101 carrying the helper plasmid pSoup and binary plasmids was grown overnight at 28°C to an optical density at 600 nm (OD_{600}) of around 0.8. Agrobacterial cells were harvested, resuspended in 10 mM $MgCl_2$, 10 mM MES-NaOH (pH 5.6), and 150 μM acetosyringone, adjusted to OD_{600} = 0.4, and incubated at 23°C for 2–3 h before infiltration. We also used the p19 silencing suppressor to enhance gene expression. For coexpression of two proteins, *Agrobacterium* carrying the appropriate two constructs and p19 helper plasmid-containing bacteria were mixed at 1:1:1 volume ratio. The uppermost 3 or 4 leaves of 4-week-old *N. benthamiana* plants were selected for injection, and inoculated plants were kept in a growth room at 25°C for 2 days.

Transient expression of Pit mutants in tobacco leaves was performed according to the method described above. Each bacterial inoculum was infiltrated in a circle with a

diameter of 1 cm on each of 15 leaves for three independent experiments. After 2–3 days, cell death symptoms became visible and were photographed.

For ROS detection and quantification assay, the infiltrated leaves expressing Pit mutants or negative control GFP were collected and floated in 1 mg/ml DAB solution for 5 h at room temperature. To visualize ROS *in situ*, the leaves were then decolorized with ethanol by boiling several times in a microwave oven until the chlorophyll was removed completely. ROS production of each sample was quantified by measuring the pixel intensities of the infected regions using ImageJ software (National Institutes of Health). The mean pixel intensity from three spots outside the infiltrated regions on each leaf was used to subtract background. Relative DAB staining intensity was calculated based on the mean pixel intensity of the GFP-infected region on each leaf to compare between different leaves.

Plant Growth and Infection

All of transgenic rice plants used in this study were produced by the core facility of Shanghai Center for Plant Stress Biology. T0 generation of transgenic plants were used for infection analysis because introduced *Pit* WT gene did not sucessfully transmit T1 generation due to unknown reasons. Nipponbare plants were grown at 30°C for 5–6 weeks before being infected with the *M. oryzae* strain Ina86-137 (Race 007.0) (Hayashi & Yoshida, 2009). Infection of leaf blades by the punch method was performed as reported previously (Ono *et al.*, 2001; Kawano *et al.*, 2010). Lesion length and fungus growth were measured at 7 dpi. Photographs of disease lesions were taken at 6 dpi.

Expression Analysis

Total RNA from rice was extracted using TRIzol reagent (Invitrogen). Total RNA (500 ng) was used for cDNA synthesis with a commercial kit (Vazyme) according to the manufacturer's protocol. The cDNA was analyzed semi-quantitatively using normal polymerase mix. Total genomic DNA was extracted by the CTAB method and then subjected to quantitative analysis using SYBR Green Supermix (Bio-Rad) on a CFX96 Touch Real-Time PCR Detection System (Bio-Rad). *OsUbiquitin* was used as an

internal control for normalization. Sequences of RT-PCR and RT-qPCR primers are listed in supplemental Table 1.

Raichu-OsRac1 FRET Analysis

The Raichu intramolecular FRET system was applied as described previously (Kawano *et al.*, 2010; Wong *et al.*, 2018). Rice protoplasts were transformed with *Raichu-OsRac1* and *Pit* mutants or *GUS* vectors by the PEG method. Images of transformed cells were captured using a LEICA SMD FLCS microscope. Raichu-OsRac1 was excited using a 440 nm solid-state laser. The Venus and CFP filters were 550 ± 25 nm and 470 ± 20 nm, respectively.

Protein Expression and Purification

His-SUMO tag- and glutathione-S-transferase (GST) tag-fused Pit CC (amino acids 1-140) were expressed in *Escherichia coli* strain BL21(DE3) Codon Plus. The bacteria were cultured at 37°C until the OD_{600} of the suspension of the medium was around 0.8. The recombinant proteins were induced with 0.3 mM IPTG for 12 h at 18°C. For protein purification, the bacterial cells were collected, resuspended, and sonicated in a lysis buffer (20 mM Tris-HCl [pH 8.0], 150 mM NaCl, 1 mM DTT). The proteins were then purified by affinity chromatography using Ni-NTA agarose resin and Glutathione Sepharose 4B resin (GE Healthcare), respectively.

***In Vitro* Pull-down Assay**

Equal amounts of His-SUMO-Pit CC and GST-Pit CC WT or mutated proteins in binding buffer (50 mM Tris-HCl [pH 7.5], 150 mM NaCl, 0.1% Triton X-100, 1 mM EDTA, and 1 mM DTT) were mixed to 200 µl for each reaction and incubated at 4°C for 5 min with gentle rotation. Glutathione Sepharose 4B resin was added to the solution for precipitation. The beads were washed five times with binding buffer and separated from the solution by centrifugation at 2500 × *g* for 2 min. The proteins were then eluted with 100 µl 2×SDS loading buffer for immunoblotting. Anti-SUMO (GenScript: A01693) and anti-GST (Abmart: M20007) antibodies were used.

873

874 **Subcellular Localization**

875 Confocal fluorescence pictures were recorded under a Leica TCS-SP8 microscope,
876 using 60×water-immersion objectives. A 488-nm laser was used to image GFP; a 514-
877 nm laser was used to image Venus; and a 598-nm laser was used to image mCherry. For
878 samples stained with a plasma membrane marker, FM4-64 (Invitrogen: F34653)
879 solution was injected to the infiltrated leaves before harvesting and observation. The
880 signals of FM4-64 were excited with a 566-nm laser.

881

882 **Luciferase Activity Assay in Rice Protoplasts**

883 Isolation of rice protoplasts and PEG transformation were performed as described
884 previously (Kawano *et al.*, 2010; Wang *et al.*, 2018). Protein preparation and luciferase–
885 substrate interaction were conducted with a Luciferase Assay Report Kit (Promega).
886 Luciferase activity was measured by a microplate reader (Thermo Scientific Varioskan
887 Flash). We used mean values of three independent replications.

888

889 **Co-immunoprecipitation Assays**

890 An *in vivo* co-immunoprecipitation (co-IP) assay was performed as previously reported
891 (Wang *et al.*, 2018). The infiltrated tobacco leaves were ground to powder in liquid
892 nitrogen and homogenized in IP buffer (50 mM Tris-HCl [pH 7.5], 150 mM NaCl, 10%
893 glycerol, 0.2% NP-40, 1 mM EDTA, 5 mM DTT, and EDTA-free protease inhibitor
894 [Roche]). Anti-GFP agarose resin (Chromotek, GFP-Trap A, gta-20) was added to the
895 extracted protein solution for precipitation. The GFP beads were washed five times and
896 then subjected to immunoblot analysis together with input samples. Anti-Myc (Cell
897 Signaling: #2276S), anti-HA (Roche: 11867423001), and anti-GFP (Abcam: ab6556)
898 antibodies were used for western blot.

899

900 **Bimolecular Fluorescence Complementation (BiFC)**

901 OsSPK1-cYFP, cYFP-OsRac1, and Pit-nYFP mutants were transiently expressed in *N.*
902 *benthamiana* leaves according to the method described above. The signals of YFP were

observed under a Leica TCS-SP8 microscope. A 514-nm laser was used to excite the YFP fluorescence and signals between 525 nm and 575 nm were recorded.

Statistical Analysis and Biological Repetitions

Means were compared by using a *t* test (two-tailed; type 2). SEs were calculated in Microsoft Excel software. All of assays (including Co-IP, Y2H, Pull down, etc.) in this study were independently repeated at least three times.

Supplemental information includes the following items:

1. Two supplemental figures and legends.

Figure S1 is related to Figure 3.

Figure S2 is related to Figure 4.

2. One supplemental table

Table S1. List of primers for experimental procedures

Figure S1. Effect of conserved hydrophobic residue mutations on Pit signaling

A, Protein expression of Pit CC WT and mutants in Y2HGold yeast cells. Anti-HA and anti-Myc antibodies were used for western blot to detect baits and preys, respectively. The post-transfer membrane was stained with Ponceau S. **B**, Quantitative analysis of the effect of I34, L37, and L41 mutation on Pit D485V-induced ROS production in *N. benthamiana*. Bars indicate DAB staining intensity relative to that observed after infiltration with negative control GFP. Data are expressed as mean ± standard error (SE) (**: $P < 0.01$; $n = 10$). Relative intensity of DAB staining (GUS=50) is shown. **C**, HA-tagged Pit mutants were transiently expressed in *N. benthamiana* leaves. After 2 days, the total proteins of infiltrated leaves were extracted for immunoblotting with anti-HA antibody. NI indicates non-infiltrated leaves. The post-transfer membrane was stained with Ponceau S and used as an internal control. **D**, Venus-tagged Pit mutants were transiently expressed in rice protoplasts. After 14 h, total protein was extracted with SDS loading buffer, and western blotting was then carried out with anti-GFP antibody. NT indicates a non-transformed sample. The post-transfer membrane was stained with

Ponceau S.

Figure S2. Three hydrophobic residues in the Pit CC domain are not necessary for binding to OsSPK1

A, Transcript levels of exogenous *Pit* WT and *Pit* mutants were measured by RT-PCR. Numbers indicate independent transgenic lines. *Ubiquitin* was used as an internal control. **B**, *In vitro* binding assay between Pit CC mutants and OsSPK1. Purified GST or GST-tagged Pit CC mutants immobilized on Sepharose were incubated with His-SUMO-tagged OsSPK1 (amino acids 1334–1835). After washing, the bound proteins were eluted by addition of SDS loading buffer. Anti-GST and anti-SUMO antibodies were used for subsequent western blotting analysis. **C**, Co-IP to analyze the interaction in *N. benthamiana* between OsSPK1 (amino acids 1002–1835) and full-length Pit with mutations in three conserved hydrophobic residues. Total protein extract was immunoprecipitated with anti-GFP antibody, and western blotting was then carried out with anti-GFP and anti-Myc antibodies. The post-transfer membrane was stained with Ponceau S.

Wang et al., Figure 1

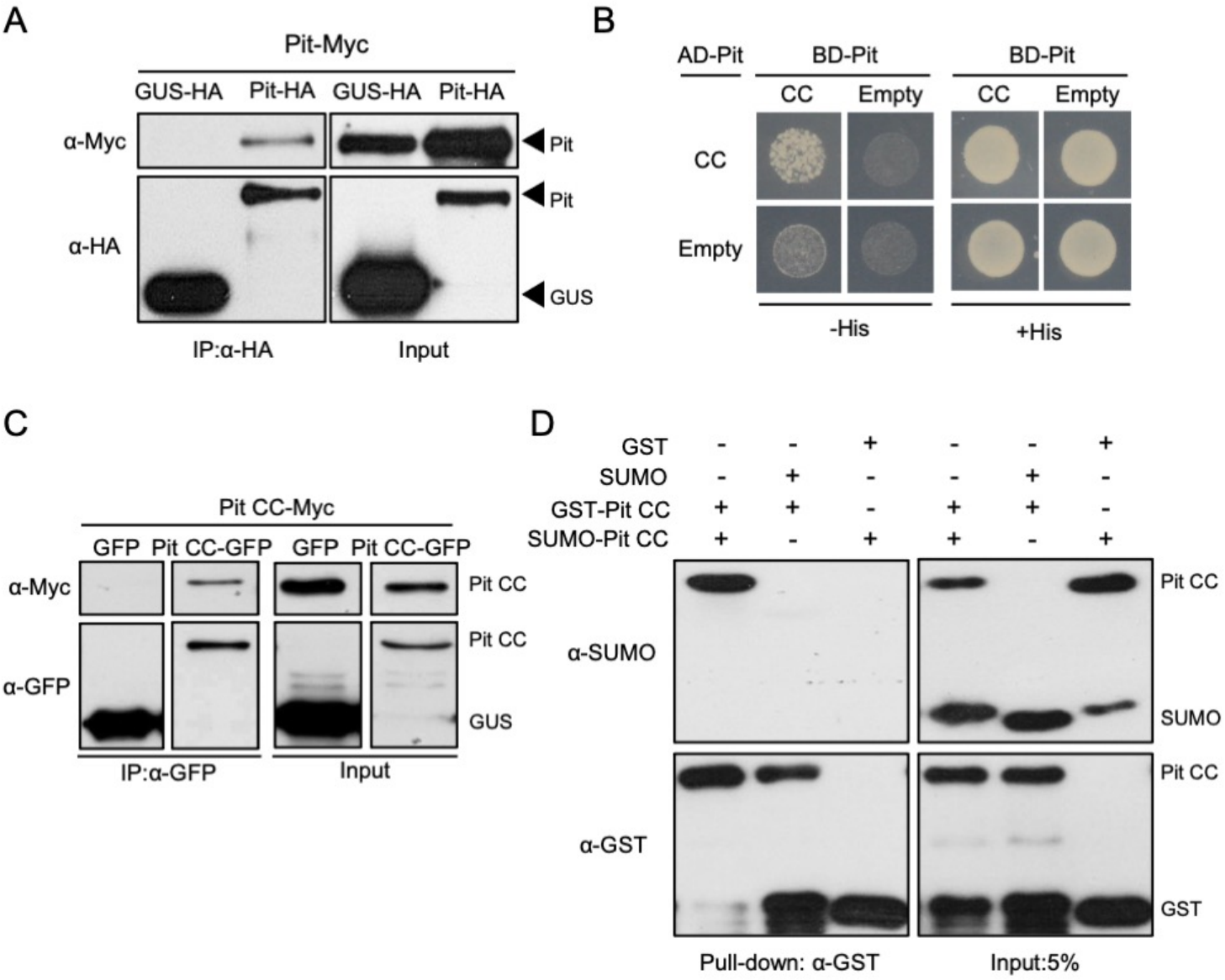

Figure 1. The CC domain and full-length Pit self-associate

A, Co-IP assay to assess self-association of full-length Pit in *N. benthamiana*. Total protein extract was immunoprecipitated with anti-HA antibody, and western blotting was then carried out with anti-HA and anti-Myc antibodies. **B**, Yeast two-hybrid assay to test self-association of the Pit CC domain. Growth of yeast cells coexpressing GAL4-AD or GAL4-BD fused with the CC domain of Pit on selective medium without histidine (-His) represents a positive interaction. AD: GAL4 activation domain, BD: GAL4 DNA-binding domain. **C**, Co-IP assay to assess self-association of the Pit CC domain in *N. benthamiana*. Total protein extract was immunoprecipitated with anti-GFP antibody, and western blotting was then carried out with anti-GFP and anti-Myc antibodies. **D**, GST pull-down assay to verify the self-association of the Pit CC domain. Purified GST or GST-tagged Pit CC immobilized on Sepharose was incubated with His-SUMO-tagged Pit CC. After washing, the bound proteins were eluted by addition of SDS loading buffer for immunoblotting with anti-GST and anti-SUMO.

Wang et al., Figure 2

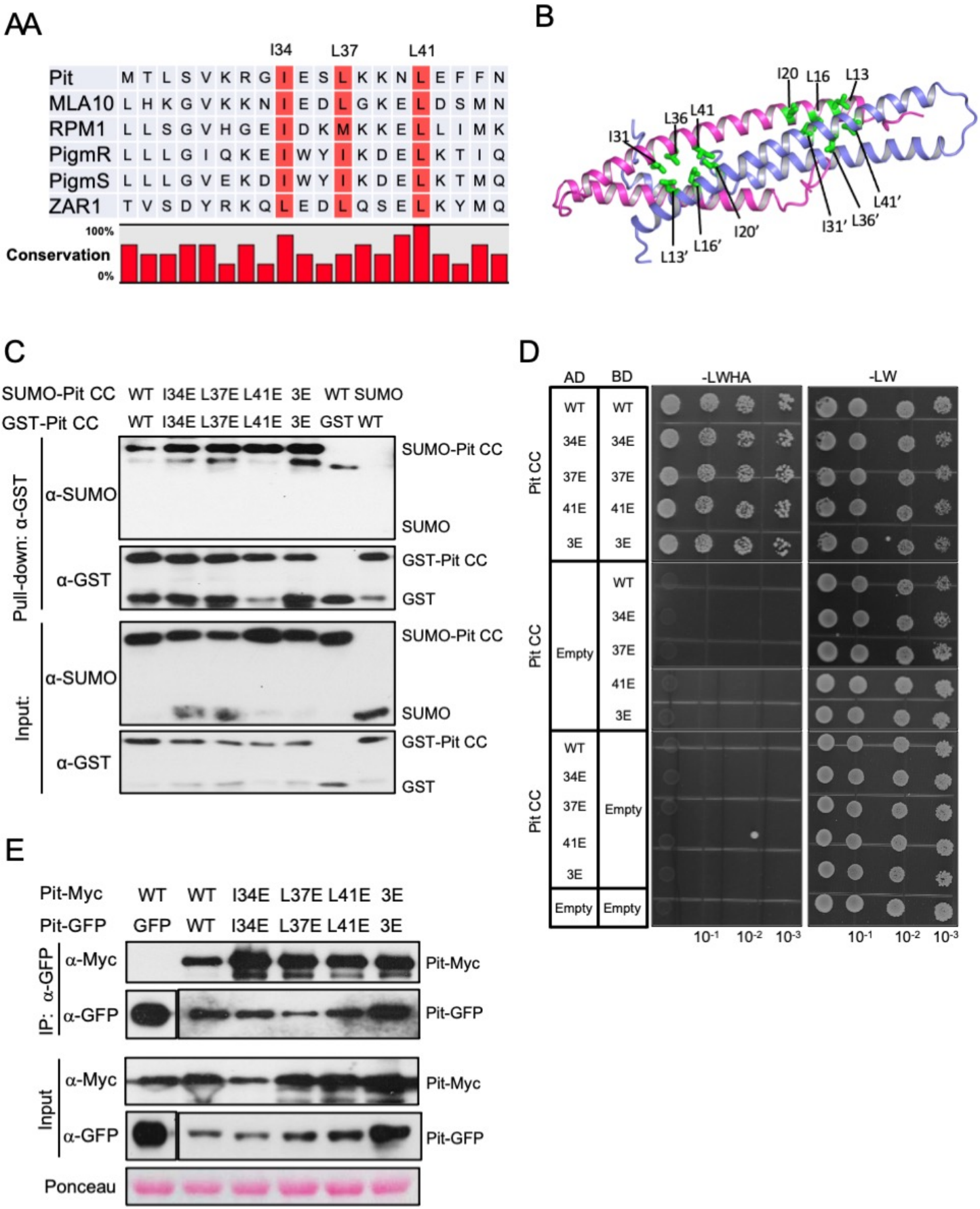

Figure 2. Conserved hydrophobic residues in the Pit CC domain are not involved in Pit self-association

A, Multiple alignment of Pit with various CNLs. **B**, Model structure of the Pit CC domain, based on the MLA10 CC domain (Protein Data Bank ID code 3QFL), shows the elongated dimer (blue and pink), stabilized by hydrophobic residues (I34, L37, and L41). The figure was drawn using PyMOL. **C**, *In vitro* pull-down assay to test the self-association of Pit CC mutants. Purified GST or GST-tagged Pit CC mutants immobilized on Sepharose was incubated with His-SUMO-tagged Pit CC mutants. After washing, the bound proteins were eluted by addition of SDS loading buffer for immunoblotting. Anti-GST and anti-SUMO antibodies were used for western blotting. **D**, Yeast two-hybrid assay to test self-association of Pit CC mutants. Growth of yeast cells coexpressing GAL4-AD or GAL4-BD fused with the CC domain of Pit on selective medium (-LWHA) represents a positive interaction. 10^{-1}, 10^{-2}, and 10^{-3} indicate dilution ratio. **E**, Co-IP assay to examine self-association of full-length Pit mutants in *N. benthamiana*. Total protein extract was immunoprecipitated with anti-GFP antibody, and western blottingwas then carried out with anti-GFP and anti-Myc antibodies. The post-transfer membrane was stained with Ponceau S.

Wang et al., Figure 3

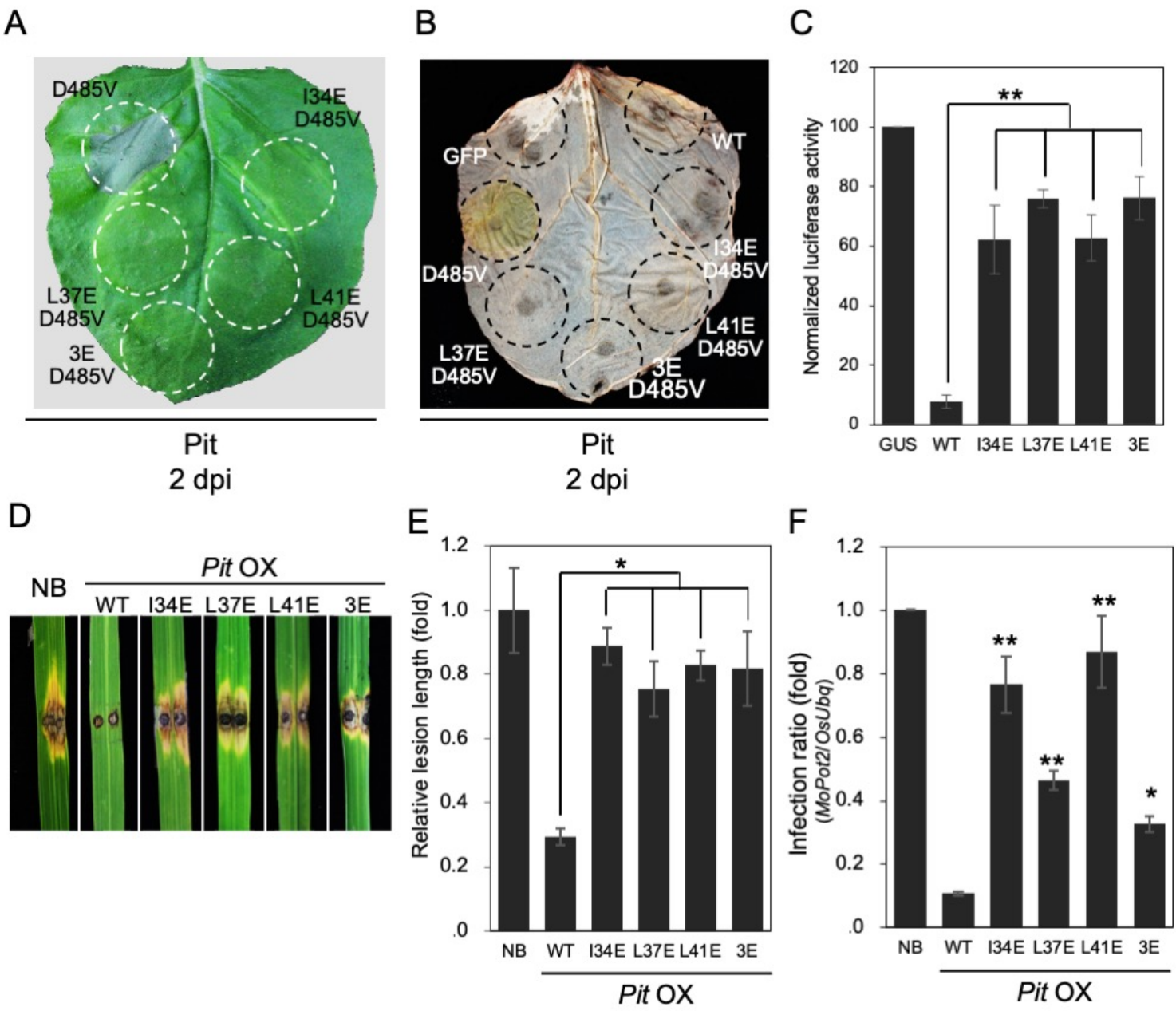

Figure 3. Conserved hydrophobic residues in the Pit CC domain contribute to Pit-mediated immune signaling
A, Cell death phenotypes induced by transient expression of Pit mutants in *N. benthamiana*. Photos were taken at 2 dpi. The circles indicate the infiltrated regions. **B**, Effect of three hydrophobic residues on Pit D485V-induced ROS production in *N. benthamiana*. ROS production was examined by DAB staining at 2 dpi. **C**, Cell death activity of Pit mutants in rice protoplasts. Relative luciferase activity (GUS=100) is shown. Data are expressed as mean ± standard error (SE) (**$P < 0.01$, $n = 3$). **D** and **E**, Responses, in plants overexpressing Pit WT or mutants, to infection with the incompatible *M. oryzae* race 007.0. **D**, Photograph shows typical phenotypes of transgenic and WT plants at 7 dpi. **E**, Statistical analysis of lesion length was performed at 6 dpi. Relative lesion length [Nippobnare (NB) = 1] is shown. Data are expressed as mean ± standard error (SE) (*$P < 0.05$; $n \geq 30$). **F**, Growth of the incompatible *M. oryzae* race in Nipponbare wild-type plants and transgenic plants overexpressing Pit WT or mutants. Relative infection ratio (NB = 1) is shown. Data are expressed as mean ± standard error (SE) (*$P < 0.05$; **$P < 0.01$; $n = 10$).

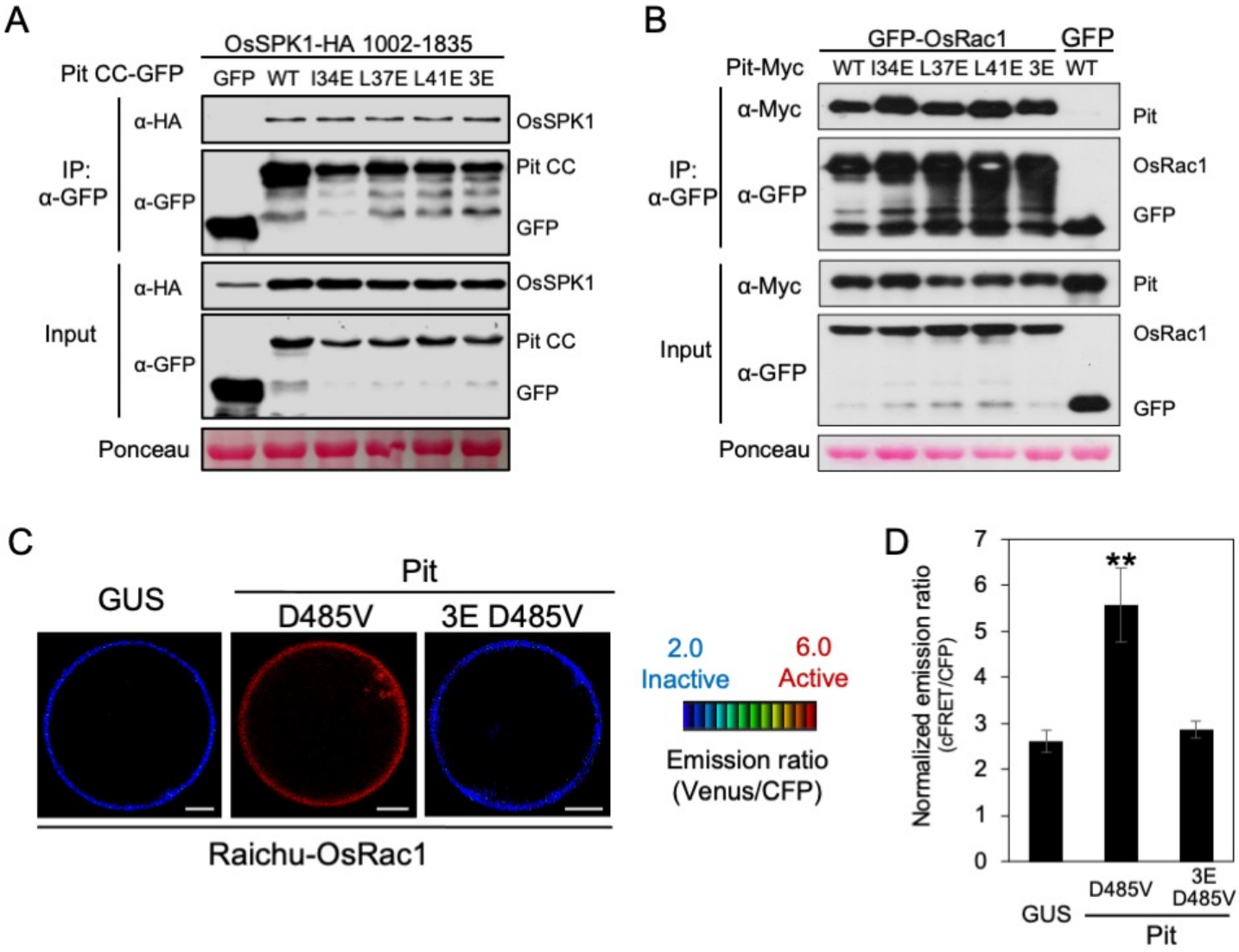

Figure 4. Mutations in three hydrophobic residues do not affect binding to OsSPK1 or OsRac1 but perturb Pit-mediated OsRac1 activation

A, Co-IP to test the interaction between OsSPK1 and Pit hydrophobic residue mutants in *N. benthamiana*. Total protein extract was immunoprecipitated with anti-GFP antibody, and western blotting was then carried out with anti-GFP and anti-HA antibodies. The post-transfer membrane was stained with Ponceau S. **B**, Co-IP to test the interaction between OsRac1 and Pit hydrophobic residue mutants in *N. benthamiana*. Total protein extract was immunoprecipitated with anti-GFP antibody, and western blotting was then carried out with anti-GFP and anti-Myc antibodies. The post-transfer membrane was stained with Ponceau S. **C** and **D**, *In vivo* OsRac1 activation by Pit hydrophobic residues mutants. **C**, Emission ratio images of confocal laser-scanning micrographs of rice protoplasts coexpressing Raichu-OsRac1 and the indicated Pit mutants, or negative control GUS. Scale bars, 5 μm. **D**, Quantification of normalized emission ratios of Venus to CFP. Data are expressed as mean ± standard error (SE) (**$P < 0.01$, $n = 60$).

Wang et al., Figure 5

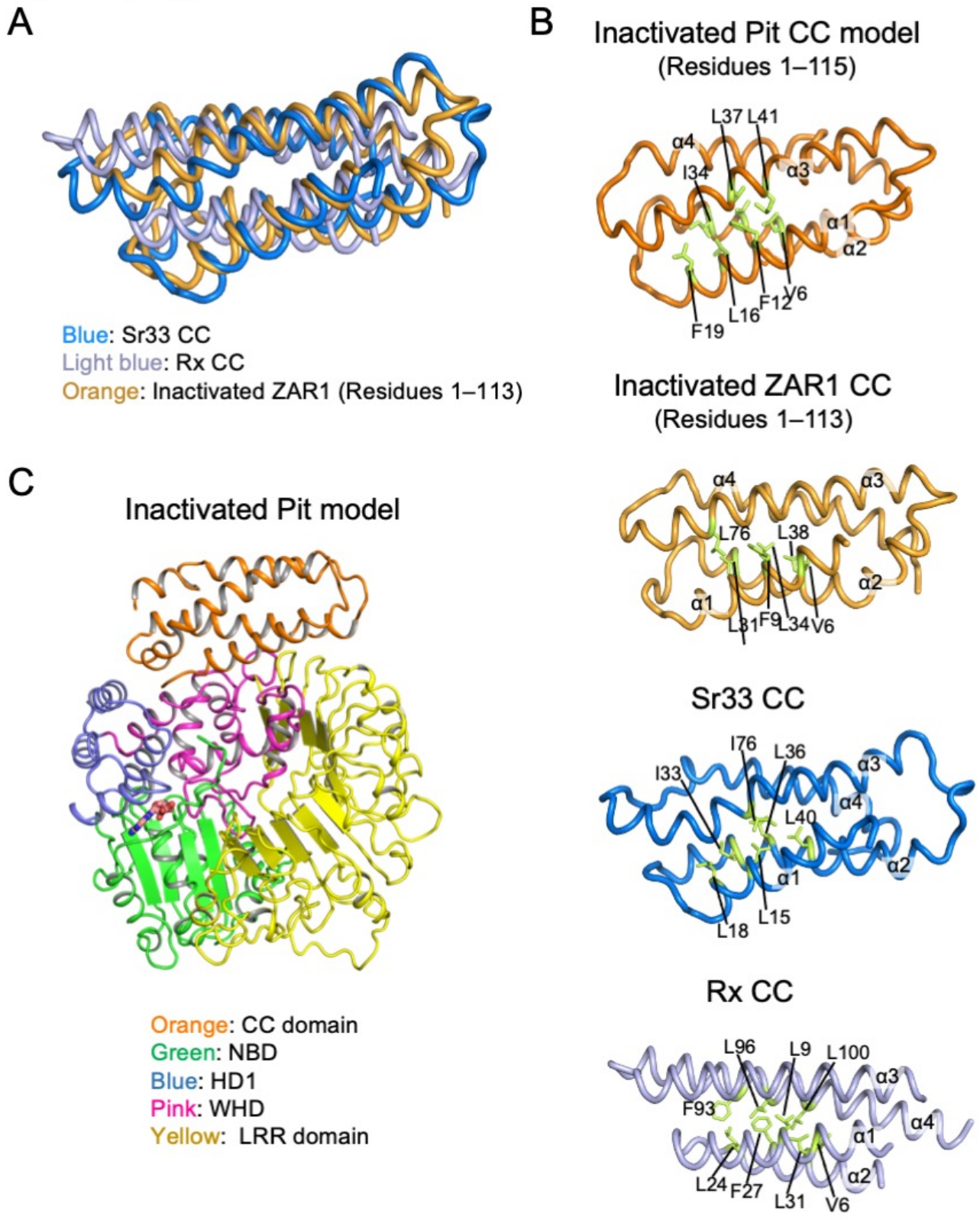

Figure 5. The CC domain of various NLRs

A, The main chains of the CC domain structure of Sr33 (blue, solution NMR condition, Protein Data Bank ID code 2NCG), Rx (light blue, crystal condition, Protein Data Bank ID code 4M70), and inactivated ZAR1 (orange, electron microscopy condition, 6J5W, residues 1–113) were superimposed using PyMOL. **B,** Comparison of conserved hydrophobic residues of Pit (residues 1–115), inactivated ZAR1 (residues 1–113), Sr33, and Rx. The side chains of three key hydrophobic residues in Pit (I34, L37, and L41) and equivalent residues in inactivated ZAR1 1–113 (L31, L34, and L38), Rx (I33, L36, and L40), Sr33 (L24, F27, and L31), as well as the side chains of amino acids thought to be involved in hydrophobic interactions with these three residues, are shown in stick representation. **C,** Model structure and domain composition of full-length Pit, based on inactivated ZAR1 (Protein Data Bank ID code 6J5W), shows the monomeric state. The figure was drawn using PyMOL.

Wang et al., Figure 6

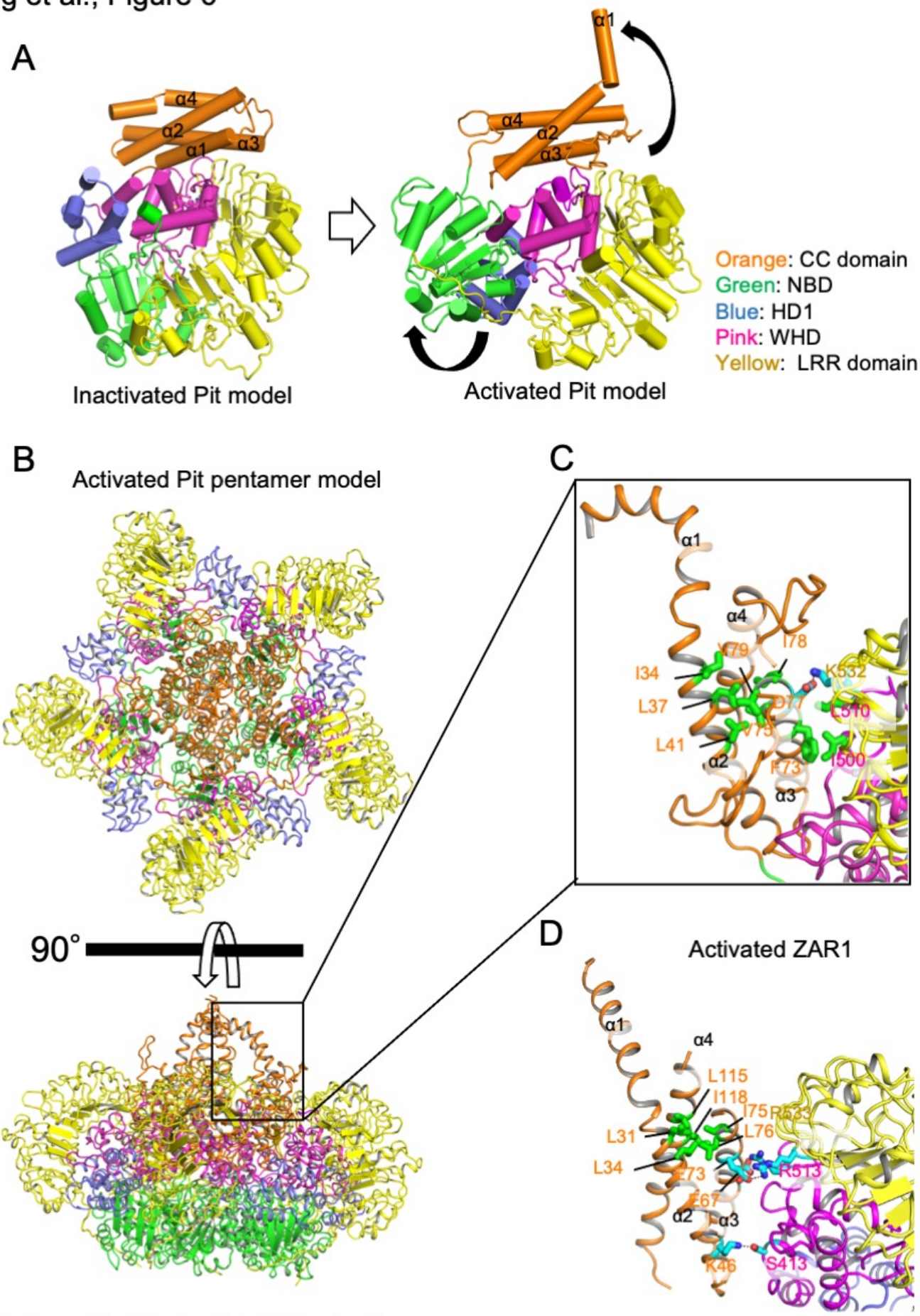

Figure 6. Homology modeling of Pit using activated ZAR1 as a template

A, Comparison of the inactivated and activated Pit model structures. The model structures of inactivated and activated Pit are based on the structures of inactivated ZAR1 (Protein Data Bank ID code 6J5W) and activated ZAR1 (Protein Data Bank ID code 6J5T). Conformational changes (black arrows) between the activated and inactivated forms of Pit occur around the hinge linking the HD domain (blue) and WHD domain (pink) of Pit and also at the α1 helix of the CC domain (orange). **B,** Model structure of the activated Pit pentamer. The extreme N-terminal α1 helix of the Pit pentamer may be required for the plasma membrane association of Pit. The CC, NBD, HD1, WHD, and LRR domains are shown in orange, green, blue, pink, and yellow, respectively. **C,** Hydrophobic interactions among α2 (I34, L37, and L41), α3 (F73, V75, I78, and V79), and WHD domain (I500 and L510) in the activated Pit pentamer model structure are shown. Residues that may be important for hydrophobic interactions in Pit function are shown in green, and hydrogen-bonded side chains are shown in light blue. **D,** Comparison of the interaction around α1 of the activated ZAR1 structure (Protein Data Bank ID code 6J5T) and the active Pit oligomer model structure. Residues involved in hydrophobic interaction around α1 are shown in green, and hydrogen-bonded side chains are shown in light blue. The figure was drawn using PyMOL.

Wang et al., Figure 7

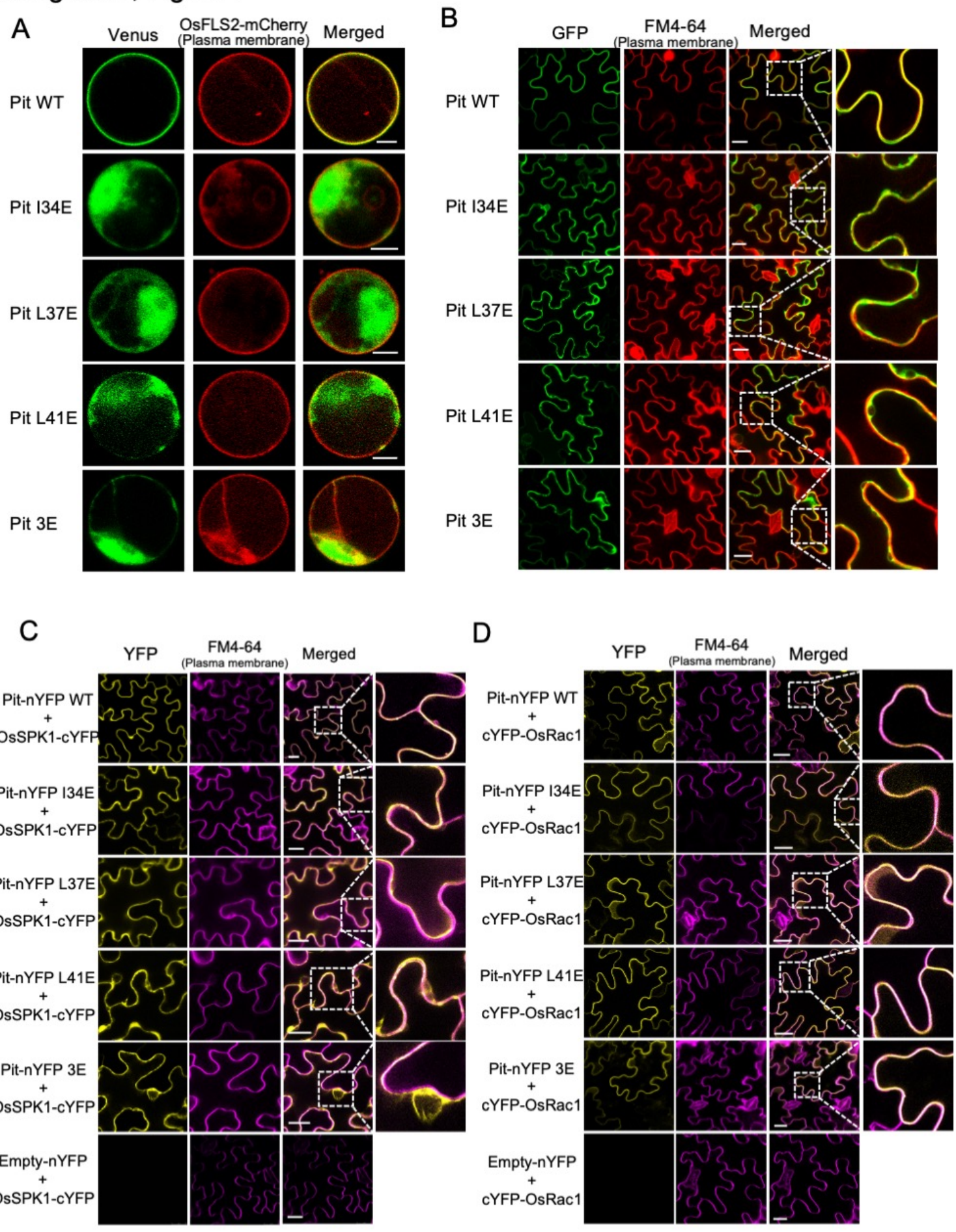

Figure 7. Mutations in the conserved hydrophobic residues of Pit influence its plasma membrane localization
A and **B**, Subcellular localization of Pit mutants in rice protoplasts and *N. benthamiana* leaves. **A**, Rice protoplasts were cotransfected with the indicated *Pit-Venus* mutants and *OsFLS2-mCherry*. Scale bars, 5 μm. **B**, Tobacco leaves were injected with *Agrobacterium* carrying *Pit-GFP* mutants (green) and stained with FM4-64 (red: plasma membrane marker). Enlarged images of the boxed areas are shown in the right panels. Scale bars, 25 μm. **C** and **D**, BiFC to detect interactions between Pit hydrophobic residue mutants and OsSPK1 (**C**) or OsRac1 (**D**). Expression constructs were transiently expressed in *N. benthamiana* after agroinfiltration. Empty vector served as a negative control. FM4-64 was used as a plasma membrane marker. Images were captured at 45 h post-infiltration. Enlarged images of the boxed areas in (C) are shown in the right panels. Scale bars, 25 μm.

Wang et al., Figure S1

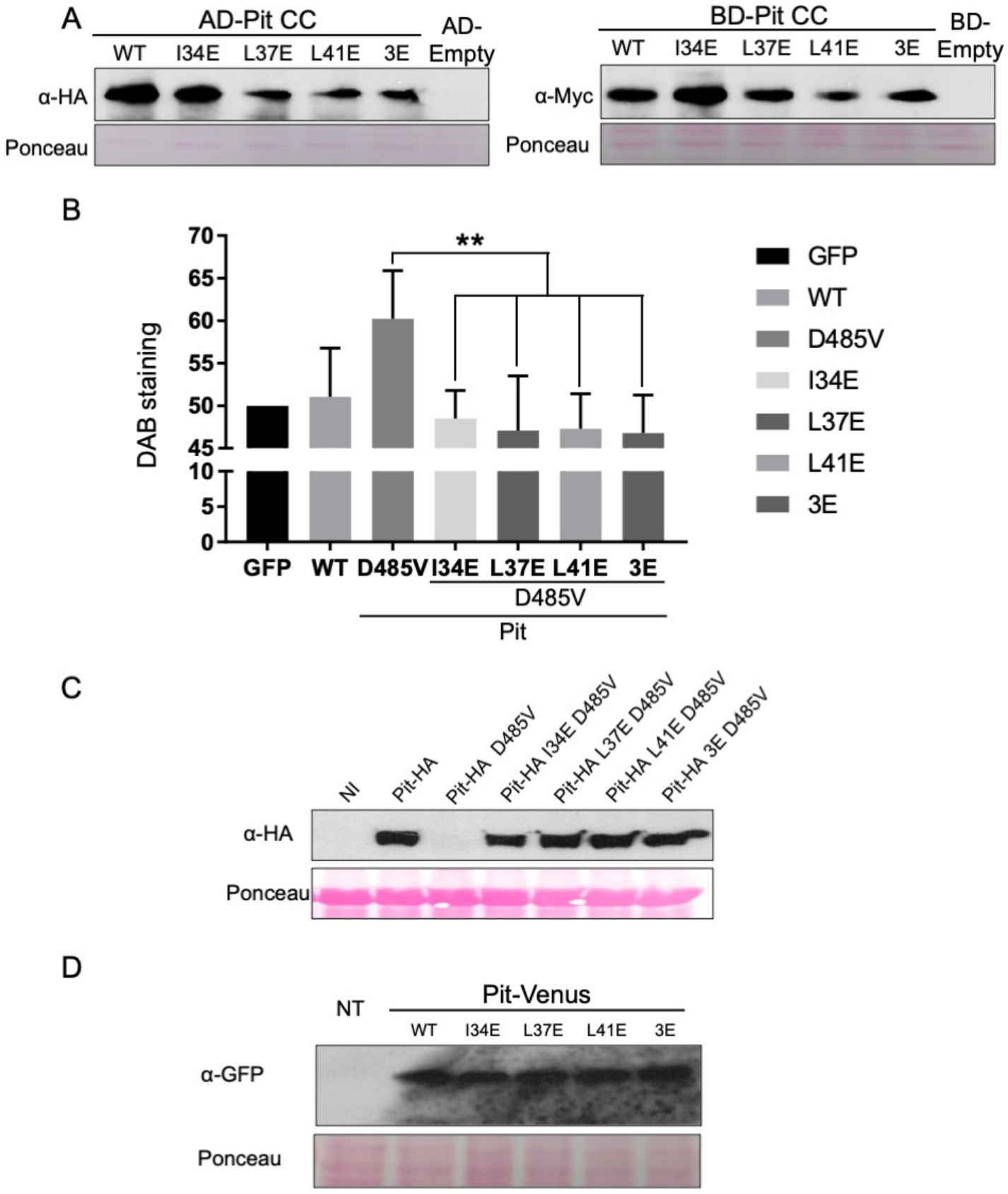

Figure S1. Effect of conserved hydrophobic residue mutations on Pit signaling

A, Protein expression of Pit CC WT and mutants in Y2HGold yeast cells. Anti-HA and anti-Myc antibodies were used for western blot to detect baits and preys, respectively. The post-transfer membrane was stained with Ponceau S. **B**, Quantitative analysis of the effect of I34, L37, and L41 mutation on Pit D485V-induced ROS production in *N. benthamiana*. Bars indicate DAB staining intensity relative to that observed after infiltration with negative control GFP. Data are expressed as mean ± standard error (SE) (**: $P < 0.01$; $n = 10$). Relative intensity of DAB staining (GUS=50) is shown. **C**, HA-tagged Pit mutants were transiently expressed in *N. benthamiana* leaves. After 2 days, the total proteins of infiltrated leaves were extracted for immunoblotting with anti-HA antibody. NI indicates non-infiltrated leaves. The post-transfer membrane was stained with Ponceau S and used as an internal control. **D**, Venus-tagged Pit mutants were transiently expressed in rice protoplasts. After 14 h, total protein was extracted with SDS loading buffer, and western blotting was then carried out with anti-GFP antibody. NT indicates a non-transformed sample. The post-transfer membrane was stained with Ponceau S.

Wang et al., Figure S2

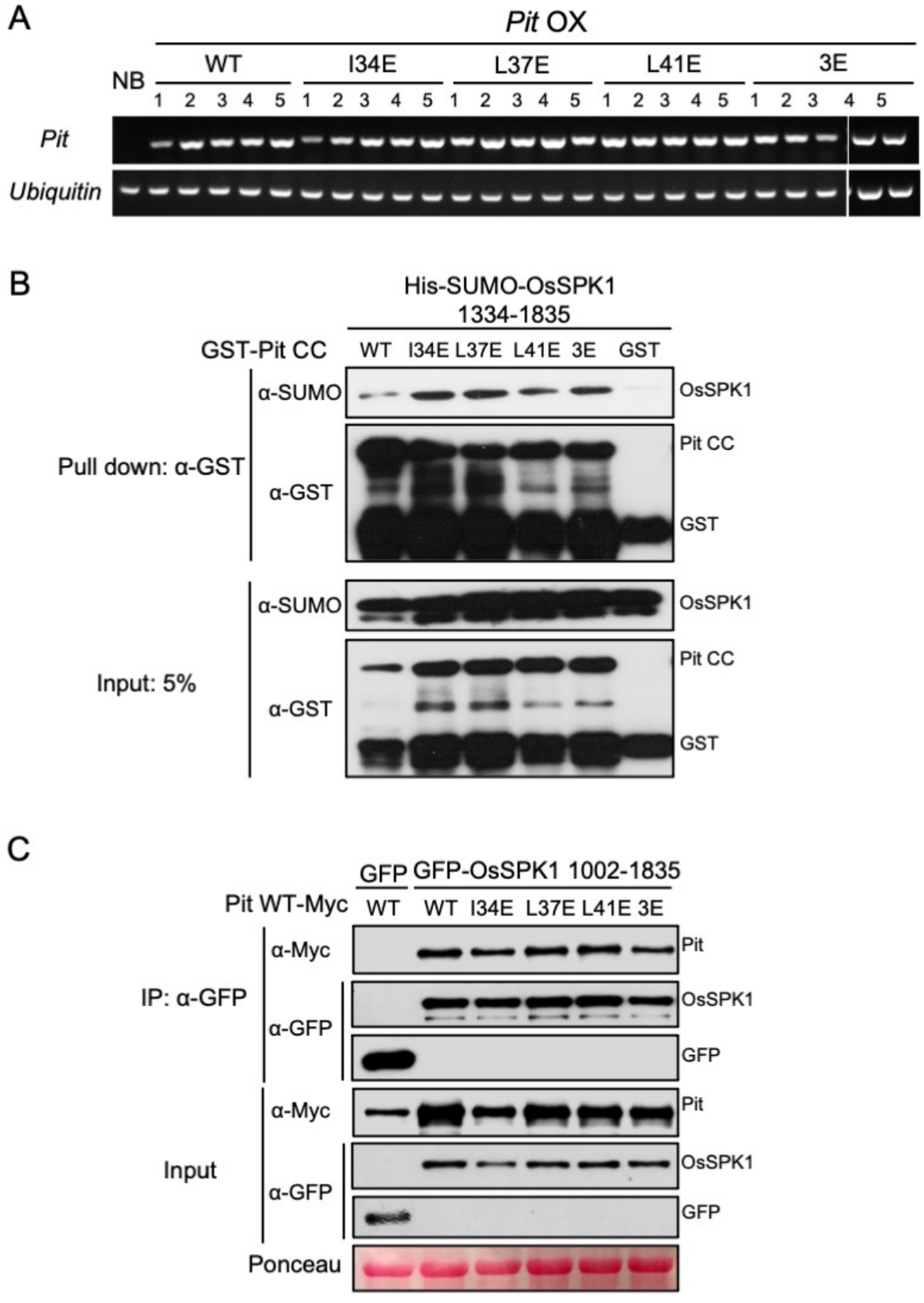

Figure S2. Three hydrophobic residues in the Pit CC domain are not necessary for binding to OsSPK1

A, Transcript levels of exogenous *Pit* WT and *Pit* mutants were measured by RT-PCR. Numbers indicate independent transgenic lines. *Ubiquitin* was used as an internal control. **B**, *In vitro* binding assay between Pit CC mutants and OsSPK1. Purified GST or GST-tagged Pit CC mutants immobilized on Sepharose were incubated with His-SUMO-tagged OsSPK1 (amino acids 1334–1835). After washing, the bound proteins were eluted by addition of SDS loading buffer. Anti-GST and anti-SUMO antibodies were used for subsequent western blotting analysis. **C**, Co-IP to analyze the interaction in *N. benthamiana* between OsSPK1 (amino acids 1002–1835) and full-length Pit with mutations in three conserved hydrophobic residues. Total protein extract was immunoprecipitated with anti-GFP antibody, and western blotting was then carried out with anti-GFP and anti-Myc antibodies. The post-transfer membrane was stained with Ponceau S.

Wang et al., Table S1

Primers for this study	
Primer name	**Sequence (5'-3')**
MgPot2-F	ACGACCCGTCTTTACTTATTTGG
MgPot2-R	AAGTAGCGTTGGTTTTGTTGGAT
UBQ-F	AACCAGCTGAGGCCCAAGA
UBQ-R	ACGATTGATTTAACCAGTCCATGA
PAL1-F	TGAATAACAGTGGAGTGTGGAG
PAL1-R	AACCTGCCACTCGTACCAAG
PBZ1-F	GGTGTGGGAAGCACATACAA
PBZ1-R	GTCTCCGTCGAGTGTGACTTG
Primers for RT-PCR	
Primer name	**Sequence (5'-3')**
Pit OX-F	CTGCACTTTGAATACCATTGGC
Pit OX-R	GGAGAATTTCCAATCTCTGTAATCTAA
Ubiquitin-F	CCAGGACAAGATGATCTGCC
Ubiquitin-R	AAGAAGCTGAAGCATCCAGC
Primers for mutagenesis	
Primer name	**Sequence (5'-3')**
Pit I34E-R	TCTTCAGGCTCTCCTCACCCCTTTTCACACTTAATG
Pit L37E-F	GTATTGAGAGCGAGAAGAAAAATCTGGAATTC
Pit L37E-R	AGATTTTTCTTCTCGCTCTCAATACCCCTTTTC
Pit L41E-F	AGCCTGAAGAAAAATGAGGAATTCTTCAACGCTG
Pit L41E-R	AGCGTTGAAGAATTCCTCATTTTTCTTCAGGCTCTC
Pit 3E-F	TGAAAAGGGGTGAGGAGAGCGAGAAGAAAAATGAGGAATTCTTCAACGCTGTTC
Pit 3E-R	TGAAGAATTCCTCATTTTTCTTCTCGCTCTCCTCACCCCTTTTCACACTTAATG